October 2018

Ice and Guano Deposits in El Malpais Lava Tubes: Potential Paleoclimate Archives for the Southwest United States

Dylan S. Parmenter
University of South Florida, dparmenter90@gmail.com

Ice and Guano Deposits in El Malpais Lava Tubes:

Potential Paleoclimate Archives for the Southwest United States

by

Dylan S. Parmenter

A thesis submitted in partial fulfillment
of the requirements for the degree of
Master of Science in Geology
School of Geosciences
College of Arts and Sciences
University of South Florida

Major Professor: Bogdan P. Onac, Ph.D.
Philip van Beynen, Ph.D.
Viorel N. Atudorei, Ph.D.

Date of Approval:
October 25, 2018

Keywords: Oxygen, Carbon, Nitrogen, Stable Isotopes, Lava Tube, Ice, Guano

Dedication

I would like to dedicate this Thesis to my loving family, Danny, Deborah, Danielle, and Jeremy, my supportive wife Cenxiao Fang, my best friends James Ledbetter, Ivan Gortinski, Avinash Mahbubani, and Brian Eshelman, as well as my fellow cavers in the Tampa Bay Area Grotto.

Table of Contents

List of Tables

List of Figures

Abstract

Three ice cores and one guano core were obtained from lava tubes in El Malpais National Monument, New Mexico, in the Southwest United States. A large hiatus in the Bat Cave guano record, resulting from mining activities in the early 1900's, left us with only ~50 years of data (from AD 1955-2006) to use in analysis. δ^{13}C values in guano (-18 to -11.6‰) primarily fall within the range of C$_4$ plants, and likely indicate a tendency of *Tadarida brasiliensis* to feed on insects over grasslands to the North or South of the park. Variations in δ^{13}C values for this period fail to reflect local temperature or precipitation influences, and are likely the result of changes in bat foraging range (to include C$_3$ plants within the park). δ^{15}N variations in Bat Cave guano (from 5.7 to 8.8‰) likely reflect changes in bat trophic level, and may also be impacted by fire activity in El Malpais. Ice cores from two lava tubes (Cave 91 and Cave 455) did not contain enough organic sediment for dating. However, analysis of LMWLs indicates that moisture from Cave 91 ice came from an arid moisture source, and strong evaporative processes were present during precipitation. The LMWL derived from Cave 455 ice closely resembles the GMWL, therefore it can be assumed that no evaporation happened during precipitation, and that the moisture came from a source of high relative humidity. The presence of abundant charcoal in Cave 29 (indicating that Native Americans melted the ice for drinking water) allowed radiocarbon dating, the results of which suggest the ice core spans the period between AD 138 and 948. Analysis of δ^{18}O from this lava tube (values range from -9.3 to -6.8‰) reveals that the majority of ice accumulation happened during summer monsoon months, with the Gulf of Mexico being the primary moisture source. A lesser degree of winter precipitation, arriving in

the form of snow storms form the Pacific, also likely contributed to ice accumulation by being deposited on the surface and percolating into the lava tube after melting in the spring. Variations in δ^{18}O in Cave 29 ice result from local surface temperature variations, with a decrease in values around AD 450 aligning with a transition from the Roman Warm Period to the Dark Age Cold Period. δ^{18}O values then display an accelerated increase beginning around AD 800, at the onset of the Medieval Warm Period. Considering the fact that ice in El Malpais caves is rapidly ablating under present day climate conditions, we highly recommend that this resource be further examined in paleoclimate studies over the next several years.

Chapter 1:

Introduction

The Southwest United States has had a history of droughts and climatic hardship long before the occurrence of large scale anthropogenic related climate changes (Grissino-Mayer, 1995; Carrillo et al., 2017). Better understanding the climate of the past few thousand years in this region not only sheds light on the struggles faced by the Native Americans and early settlers of the Southwest, but may also give us insight into the problems affecting our society in the present and near future. Paleoclimate reconstructions are generated using proxies preserved in biological or inorganic archives that maintain evidence of past climate conditions. New archives are continually sought out by researchers to obtain a more complete picture of our planet's climatic past (Lowe & Walker, 2015).

Ice cores from glaciers and ice sheets have long been a source of paleoclimate data, with oxygen and hydrogen analysis having the potential to reveal temperature records and paleo-moisture sources (Gat, 2010). The isotopic composition of cave ice was first examined by Şerban et al. (1967), and later in more detail and using modern calibration techniques by Yonge & MacDonald (1999). Its first use in paleoclimate reconstruction was in two studies of Focul Viu Ice Cave in Romania by Kern et al. (2004), and Fórizs et al. (2004). While oxygen isotopes in cave ice in El Malpais have been examined by Dickfoss (1996), a full paleoclimate record based on isotopic composition of ice has yet to be examined in New Mexico.

Guano (bat excrement) that accumulates under maternity colonies during warm seasons has been found to have great potential in carbon and nitrogen isotope analysis, revealing

1

information about past vegetation association and precipitation regimes (Marais et al., 1980; Wurster et al., 2007; Onac et al., 2014; Forray et al., 2015, Cleary et al., 2016). Fractionation in nitrogen stable isotopes in guano, being identifiable in specific conservative pathways in the bat food web, has also been demonstrated to indicate climatic variations, as well as changes in anthropogenic activities (Cleary et al., 2016).

In this study, we have obtained one guano core and three ice cores from four different lava tubes in the El Malpais National Monument. The goal of this thesis is to test the following hypotheses:

1) A previous study by Asmerom et al. (2007) on the $\delta^{18}O$ record in speleothems in New Mexico attributed isotopic variations to change in moisture sources. If large fluctuations in the $\delta^{18}O$ signal in ice from lava tubes can also be attributed to changes in moisture source, we can better determine if rainfall in El Malpais National Monument area was derived from the Gulf of Mexico or the Pacific Ocean throughout the duration of ice accumulation for our chosen cores.

2) In a study by Marais et al. (1980) it was found that when carbon enters the bat food web, it carries with it an isotopic signal specific to a particular photosynthetic pathway representative of either C_3, C_4, or CAM plants. If $\delta^{13}C$ values in guano reflect various photosynthetic pathways in local vegetation, we can track changes in dominant vegetation type in the region near a given cave that in turn provides a hydroclimate record or documents different water use efficiency (Farquhar et al., 1982).

3) Robinson (2001) found that $\delta^{15}N$ could be used as an integrator for variations in the Nitrogen Cycle. Based on work by Bird et al. (2007), Wurster et al. (2015), and Cleary et al. (2016), if it can be assumed that $\delta^{15}N$ trends in the bat-food web reflect changes in the Nitrogen Cycle, then we may use the values from our guano core to make assumptions about past anthropogenic activities, precipitation, and fires in El Malpais.

Chapter 2:

Background

2.1 Study Area

2.1.1 Geological Settings of El Malpais National Monument

El Malpais is one of two volcanic fields on the Colorado Plateau, the other being the Sunset Crater Region located in Arizona. The El Malpais lava field is part of the greater Zuni-Bandera volcanic field, which also includes the Northern and Southern Chain of craters to the West. The Zuni-Bandera volcanic field has one of the longest spanning volcanic histories in the United States, estimated to range from 700,000 to 3,000 years ago (Laughlin et al., 1994). Most of the defining features of El Malpais can be attributed to multiple lava flows creating new surfaces every 7,000-25,000 years (Mabery, 1997). Figure 1 displays a map of El Malpais National Monument and its location in the United States.

The primary stage of volcanism found in El Malpais can be characterized as having three main basalt variations: tholeiitic, alkalic, and transitional (Ander, 1997). The oldest volcanic activity in El Malpais is attributed to the El Calderon flow discovered by Maxwell (1986), which has been dated through K-Ar methods to be around 91 ka (Laughlin et al., 1993). Newer volcanic activity is characterized by the Lava Crater Flow, dated at 17 ka by Dunbar and Phillips (1994), and the McCartys Flow, the youngest flow in El Malpais at 3 ka (Maxwell, 1986; Laughlin et al., 1994).
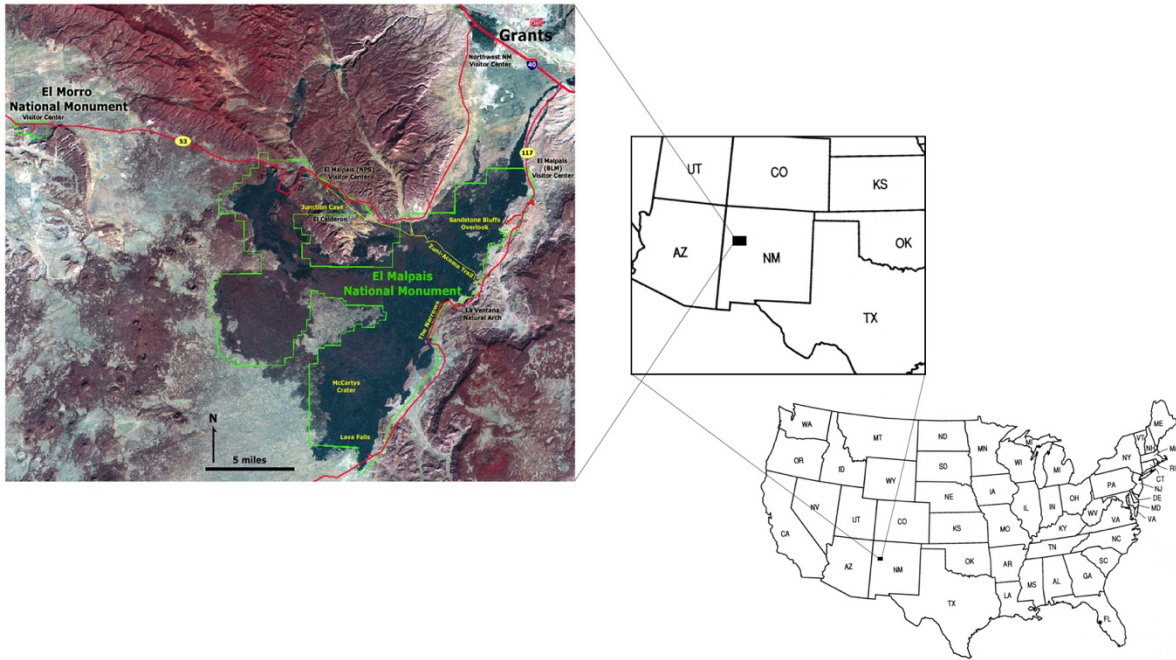
Figure 1: A map of the El Malpais and El Morro National Monument and its location in the continental United States (USGS, 2017).

2.1.2 Lava Tube Formation and Morphology

A lava tube can be described as a type of cave that forms in lava flows where the roof solidifies faster than the middle section, allowing it to empty out and leave a system of tube-shaped cavities (Rogers & Mosch, 1997). There are 457 documented lava tubes in El Malpais National Monument, in which at least 14 different species of bats make their homes (NPS, 2015a). Since some of the lava tubes used in this study are closed to public access, for safety and conservation reasons, cave numbers provided by NPS will be used in place of names.

Conditions important to the formation of lava tubes include moderate effusion rates, eruptions lasting more than two days, and fluid lava that has not significantly degassed such as pahoehoe (Greeley, 1987). Both Aa and Pahoehoe flows can be found in El Malpais (Fig. 2), the majority of which are composed of basalt. This petrology and type of flow (Aa) is important in

the formation of lava tubes, as basalts solidify much faster than other magmas when in contact with air. This leads to the development of a crust (future lava tube roof) at the surface that has the potential to insulate the lava flowing beneath, sustaining the higher temperatures necessary to extend flow distances (Rogers & Mosch, 1997). Lava tubes generally start out with elliptical morphologies, but can evolve into more circular cross sections as the crust cools from the outer walls towards the interior (Kauahikaua et al., 1998).

A lava tube with a collapsed entrance in the upper section and deeper descending sinuous passages has the potential to form a cold air trap. While ice deposits in most caves will experience melting during warm seasons, caves that act as cold air traps will hold cool air during the summer as the higher density of cold air keeps it from escaping to the surface. As the outside air temperature becomes lower than that of the cave interior in the fall, convection will resume and cooler air will sink to the lower passages (Perşoiu & Onac, 2018). The underlying processes involved in cave ice formation are discussed in further detail in section 2.4.1.

Figure 2: Aa (**left**) and Pahoehoe (**right**) flows in El Malpais (left photo courtesy BP Onac).

2.1.3 Cave 91

The entrance to Cave 91 (2353 m asl) is a collapsed lava tube ceiling with a ~12 m drop that must be rappelled down for access (Fig. 3). The lava tube has a total surveyed length of 145.2 m, and is 41 m below surface at its deepest point. Because of the difficult access, the lava tube interior has remained undisturbed by anthropogenic activity. The relative humidity measured by NPS employees in the main ice room between January and September 2017 indicates an average of ~95%. The air temperature inside the cave for 2017 averaged -0.88$^{\text{o}}$C.

Figure 3: Image of the collapsed entrance that gives access to Cave 91 (photo courtesy BP Onac).

2.1.4 Cave 455

At an altitude of 2268 m, the entrance to Cave 455 is a difficult to find small hole on the

side of a large collapsed lava tube. The ice block inside this cave extends from floor to the

ceiling and is ~1.2 m in thickness. The tube has a total surveyed length of 113.8 m and a depth

of 23.4 m. No temperature or humidity records are available for this site.

2.1.5 Cave 29

Cave 29 (Fig. 4) opens at the same altitude as Cave 455. It is a portion of a larger lava

tube with a long collapsed ceiling entrance dividing it into two sections. The tube has a

horizontal length of 146.6 m and a depth of ~12 m. No temperature or relative humidity

measurements were conducted in Cave 29. Large mounds of charcoal line the section of the tube

containing the ice block, and some pottery can be found as well. It is possible that ice was mined

from this tube by Native Americans, or later by settlers from the 1800s.

Figure 4: The collapsed entrance into Cave 29 viewed from inside.

2.1.6 Bat Cave

Bat Cave (Fig. 5) is located just east of the El Calderon Crater. It is home to at least 2 species of bats that use the cave as maternity or hibernation site, being currently closed in the interest of public health and bat conservation. Around 50,000 Mexican free-tailed bats (*Tadarida brasiliensis*) form maternity colonies along the lava tube during the spring-summer and migrate south for the winter months (NPS, 2015a). A small population of between 10-20 Townsend's big eared bats (*Corynorhinus townsendii*) makes its home in Bat Cave during the winter months for hibernation (Weaver, pers. comm., 2018).

Figure 5: The entrance to the Bat Cave (USGS, 2017).

2.1.7 *Tadarida brasiliensis* Dietary Habits

The maternity colony found in Bat Cave consists of only *Tadarida brasiliensis*, and we must take into consideration their diet when tracking carbon and nitrogen isotope signal variations in the bat food web. *Tadarida brasiliensis* is insectivorous, with a diet consisting primarily of *carabidae* (ground beetles), *lygaeidae* (milkweed bugs) in the evenings, and

lepidoptera (butterflies and moths) in the mornings, as reported in a study in Mason County, Texas (Whitaker et al., 1996). The same study found that smaller amounts of *Scarabaeidae* (scarab beetles), other species of *coleoptera* (beetles), *cicadellidae* (leaf hoppers), and *cydnidae* (burrowing bugs) are also included in their diet. In a study by Davis et al. (1962) in Texas, it was found that *Tadarida brasiliensis* tend to stay within ~80 km of their cave in any given foraging trip.

2.2 Modern Climate Setting of Southwest United States

2.2.1 Temperature

Temperature in the Southwest US follows a normal four season cycle with maximums in the summer and minimums in the winter, decreasing with higher elevations (Sellers & Hill, 1974). El Malpais experiences a broad range of temperatures throughout the year, with daily high and low differences of up to 16.65^oC (30^oF). The park typically sees summer highs in the mid-30's (~95^oF), and nights in the winter reaching temperatures as low as -29^oC (-20^oF) (NPS, 2015b).

2.2.2 Precipitation

The Southwest US, being located south of the average winter westerly storm tracks, is usually not subject to the large amount of precipitation brought to the northern states during these months. Rather, these westerly storms result in higher winds and increased cloud cover throughout the area. When precipitation does occur in the winter, it is often caused by large cyclones spanning a few thousand kilometers that enter North America via California. Large variations in winter climate in the Southwest US can be attributed to 4 major causes: the Pacific/North American (PNA) pattern, Southwestern troughs, the El Niño-Southern Oscillation (ENSO), and the Pacific Decadal Oscillation (Sheppard et al., 1999). A positive PNA pattern

results in an eastward shift of the exit region of the East Asian jet stream, while a negative PNA pattern forces a westward retraction (NOAA, 2012). In the Southwest US, a positive PNA pattern can also be linked to above average precipitation depending on the location of the east to west high-pressure ridge, where a negative pattern will usually result in below average precipitation (Simmons et al., 1983). During Southwestern troughing, a phenomenon in which meridional flow is displaced westward, the winter circumpolar vortex grows and pushes Pacific storms to the south, causing them to absorb more moisture and contributing to a large increase in precipitation in the Southwest US (Sellers & Hill, 1974).

The dominant feature of summers in the Southwest US is the North American Monsoon System (NAMS), which develops from the thermal contrast between continents and oceans in low-latitude regions, and has a large effect on warm season precipitation patterns (Sheppard et al., 1999). NAMS has a strong effect on most of the western United States as well as northwestern Mexico, the onset of which typically occurs in Mexico in June, and later in higher latitudes such as in New Mexico and Arizona (Higgens et al., 1997).

The moisture source of NAMS has long been a point of controversy in the Paleoclimate Community. Early theories by Bryson & Lowry (1955) and later corroborated by Sellers & Hill (1974), pointed to the Gulf of Mexico as the primary source of moisture. Hales (1974), on the other hand, proposed a model in which NAMS moisture flux could be traced to the Gulf of California. In the National Centers for Environmental Prediction (NCEP) and the National Center for Atmospheric Research (NCAR) reanalysis, a climate dataset created by the NCEP-NCAR, Higgens et al. (1997) found that moisture sources of water vapor in the Sonora Desert (Arizona), could be divided into lower and upper levels, with moisture below 850 hPa coming from the Gulf of California and moisture above 850 hPa originating in the Gulf of Mexico. This

was roughly in agreement with a European Centre for Medium-Range Weather Forecasts (ECMWF) analysis by Schmitz & Mullens (1996), which separated the primary moisture sources at 700 hPa.

Other studies seeking to understand moisture sources in the Southwest US have focused on stable isotope behavior. Oxygen and hydrogen isotopes from the Gulf of Mexico and Pacific Ocean have specific values and are preserved in multiple archives, including ice, speleothems, fossils, lake sediments, and tree rings. Summer moisture in New Mexico has been found to be more isotopically heavy (positive), representative of moisture from the Gulf of Mexico, whereas the winter precipitation bears a lighter (negative) isotope signal closer to that of the Pacific (Hoy & Gross, 1982; Yapp, 1985).

The ENSO is the primary driver for major weather pattern changes in the spring/autumn dry seasons of the Southwestern US climate (Kiladis & Diaz, 1989). During El Niño events, both spring and autumn see an atypical increase in precipitation due to unusually warmer water from the West Coast, which enables the creation of powerful west-coast troughs and decreases the magnitude of tradewind inversion (Andrade & Sellers, 1988). The effects of ENSO on summer precipitation are minimized, primarily due to the fact that the NAMS supplies a fairly constant influx of precipitation (Sheppard et al., 1999). While the effects are largely diminished in the winter by mid-latitude storm systems (Andrade & Sellers, 1988), stronger ENSO events can result in variations in cold season precipitation. Large, warmer ENSO events (El Niño) lead to cooler winters with increased precipitation, with deserts in the Southwest US experiencing winter flooding. Strong cold ENSO events (La Niña), on the other hand, result in a negative PNA pattern, which causes warmer, more arid climate conditions during cold seasons (Kiladis & Diaz, 1989).

11

2.2.3 Droughts and Megadroughts

The Southwest US owes much of its aridity to a semi-permanent subtropical high-pressure ridge, which spans the climate region; other contributing factors include above average temperatures, rain shadow effects from nearby mountains, and the related increase in evapotranspiration (Scott, 1991). Droughts in the Southwest US can be particularly intense, sometimes spanning several decades (Fig. 6). In one study by Carrillo et al. (2017), the past century of drought data was analyzed using tree ring time series complimented with the Twentieth-Century Reanalysis product (20CR). Their study found that the majority of multiyear drought and pluvial events could be linked to ENSO, with El Niño like conditions consistent with droughts and La Niña phases coinciding with pluvials. The largest drought found in their study spanned between AD 1912 to 1933.
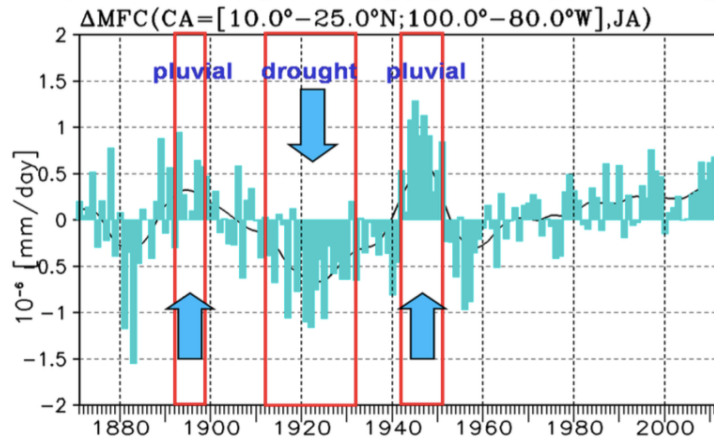
Figure 6: The July-August (JA) Moisture Flux Convergence (MFC) anomaly time-series. The convergence and divergence of the moisture flux are pointed out with arrows. The dotted bars show annual changes and the solid line represents the running mean over 10 years (Carrillo et al., 2017).

2.3 Oxygen and Hydrogen Stable Isotope Analysis in Paleoclimate

2.3.1 Basic Principles and Delta Notation

Any of two or more species of the same chemical element having the same number of protons but a different number of neutrons is called an isotope. The majority of elements have multiple naturally occurring isotopes (stable or radioactive), with the exception of 21 "monoisotopic" elements (Sharp, 2007). Stable isotopes are so named because they do not decay into other elements. In contrast, all unstable (radioactive) isotopes decompose spontaneously in time, ultimately achieving a stable nuclear composition. Oxygen has three naturally occurring stable isotopes, ^{16}O, ^{17}O, and ^{18}O, with ^{18}O being the more abundant of the two heavier isotopes (Gat, 2010). Naturally forming hydrogen stable isotopes consist of H^1 (Protium), and H^2 (Deuterium) (Sharp, 2007).

The main principle behind the use of oxygen stable isotopes in paleoclimate reconstructions is based on the fact that oxygen isotopic variations (heavy to light oxygen isotope ratio) in ice (in our case) reflect changes in the isotopic composition of meteoric water and can be linked to climate through the understanding of the hydrologic cycle (Bradley, 2015). When ocean water evaporates, the lighter oxygen isotope (^{16}O) will be preferentially removed before the heavier isotope (^{18}O) (Gat, 2010). The various processes that lead to preferential fractionation are discussed in further detail in section 2.3.3.

There are two main types of fractionation that occur in nature, equilibrium and kinetic. Equilibrium processes can be described as those in which isotope behavior is related to bond strength (Sharp, 2007). For example, when water condenses, the liquid phase has stronger bonds than those in gas, and the heavier oxygen isotope will condense before the lighter one. Kinetic processes describe irreversible and fast reactions, and are more common in biological processes

13

such as photosynthesis and microbial activity, and are governed not by bond strength, but by the reaction speeds of isotopes (Gat, 2010). They can also occur in non-organic natural processes such as evaporation and diffusion.

The isotope ratio values in samples (R_{sample}) are then compared to those in a standard ($R_{standard}$). The most commonly used standard for oxygen isotopes is the Vienna Standard Mean Ocean Water (VSMOW) (Clark & Fritz, 1997). The result of this comparison is expressed in delta notation as shown below

$$\delta^{18}O = 1000 \times \frac{^{18}O/^{16}O\,sample - \,^{18}O/^{16}O\,standard}{^{18}O/^{16}O\,standard}$$

,

where $\delta^{18}O$ is expressed in per mil (‰). In paleoclimatology, $\delta^{18}O$ in ice sheets can be described as having a positive relationship with global temperatures; that is, a ^{16}O-enrichment in ice due to a decrease in temperature results in lower $\delta^{18}O$ values relative to those of the ocean (Gat, 2010).

2.3.2 Local Meteoric Water Lines

The average oxygen and hydrogen stable isotope ratios in meteoric waters are expected to have a linear relationship, described by the so-called Meteoric Water Line. A Local Meteoric Water Line (LMWL) can be established for a specific location and its equation is then compared to the one of the Global Meteoric Water Line (GMWL) of non-evaporated meteoric water (Gat, 2010).

$$\delta^2H = 8 \cdot \delta^{18}O + 10\ (‰)$$

This equation was modified to a long-term weighted means through analysis of all available International Atomic Energy Agency (IAEA)/World Meteorological Organization (WMO) station data by Rozanski et al. (1993):

$$\delta^2H = (8.20 \pm 0.07)\,\delta^{18}O + (11.27 \pm 0.65)\ (‰),$$

14

where variations in slope are primarily determined by the extent of evaporation during precipitation, and changes in the intercept, also referred to as deuterium-excess (d-excess or simply d), represent variations in environmental conditions such as humidity and temperature at the moisture source (Craig, 1961).

By algebraically modifying the GMWL equation, d-excess has been defined by Dansgaard (1964) as:

$$d = \delta^2 H - 8 \cdot \delta^{18} O$$

As suggested by Rozanski (1987) and later confirmed by Froehlich et al. (2002), d-excess has an inverse relationship with relative humidity at moisture sources. This accounts for changes in d-excess with seasonality, when a decrease in d-excess is attributed to an increase in humidity over the ocean relative to humidity over continents.

2.3.3 Oxygen and Hydrogen Isotope Fractionation in Precipitation

After evaporating from sea water, oxygen and hydrogen isotopes are subjected to further fractionation processes (Fig. 7). For example, as moisture moves over regions of higher altitude, the decrease in temperature causes condensation and "rain out", leaving air masses further enriched in the lighter isotopes. This is known as the *altitude effect* and only holds true for liquid precipitation (Gat, 2010). In one study, the specific oxygen isotope variations due to the altitude effect for different regions were estimated, with variations in North America approximating -0.27‰ for every 100 m of altitude (Poage & Chamberlain, 2001). Following this model, with the lava tubes of our study area being located at an average altitude of ~2296 m, we should expect a decrease in oxygen isotopes due to the altitude effect.

Oxygen isotopic fractionation in the atmosphere can also be attributed to the so-called *latitude effect* (Gat, 2010). As latitude increases, $\delta^{18} O$ and $\delta^2 H$ values will decrease. The IAEA

has estimated this effect in North America as a -0.6‰ decrease in δ^{18}O for each degree increase in latitude. Since the study region, at a latitude of 35°, is roughly 5° north of the Gulf of Mexico, we expect a decrease in δ^{18}O due to the latitude effect (IAEA & UNESCO, 2001).

Other processes contributing to variations of the isotopic composition include the amount and continental effects. The *amount effect* describes a decrease in δ^{18}O values due to increased rainfall (Fritz & Clark, 1997), and while it is typically for tropical and sub-tropical regions and only a factor in summer precipitation for the mid-latitude climate belt, the low amount of rainfall and high air temperature above the exposed basalt fields in the El Malpais area could make it relevant to our study. The *continental effect*, relates to a decrease in δ^{18}O values as moisture moves inland from the coast. It is extremely variable by region and difficult to account for without in-depth modeling of evapotranspiration and moisture flux by season for the specific region in question (IAEA & UNESCO, 2001).
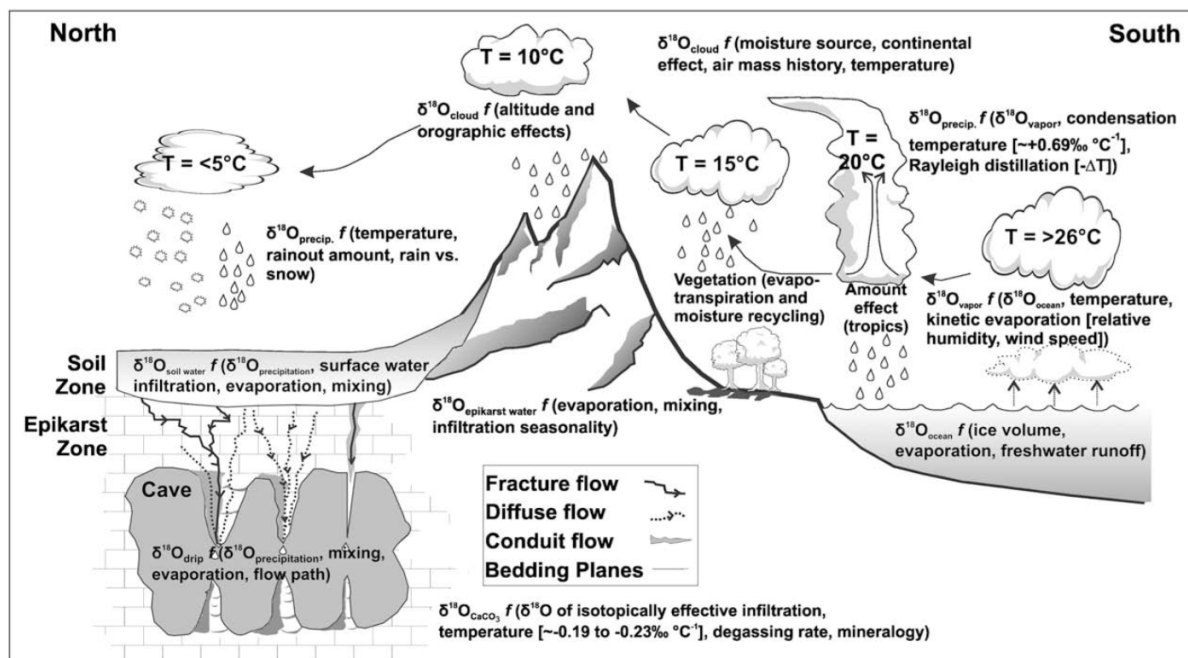
Figure 7: A diagram of the various fractionation factors for oxygen as it travels from moisture source to caves (Lachniet, 2009).

2.4 Ice in Caves

Ice caves refer to rock caves containing perennial ice and are totally different from glacial

caves, which are cavities solely developed in glaciers. Ice cave can be found in many countries

around the world, with the likelihood of occurrence increasing with higher latitudes (Perşoiu &

Lauritzen, 2018).

2.4.1 Models of Cave Ice Formation

In a recently published book, Perşoiu & Lauritzen (2018) argue that the primary

prerequisite for glaciation in caves is that the temperature of the rock remains negative yearlong.

At lower latitudes, such as in the El Malpais (~35°N), specific conditions are required to

maintain negative temperatures inside caves during warm seasons.

Perşoiu & Onac (2018) recognized three main mechanisms for cave ice formation: 1)

trapping of snow, 2) ventilation due to the chimney effect, and 3) the presence of cold air traps.

The freezing of melt water in a trapped snow pack is a possible method of ice accumulation, but

there are currently no studies that detail this process. The chimney effect, a far more common

phenomenon, is possible in caves with two or more entrances at varying elevations. The

temperature difference at these entrances results in a pressure gradient at the lower entrance,

advecting cold air and expelling warm air through the upper entrance in cold seasons. During

warm periods, this circulation is reversed with cold air entering via the upper entrance and warm

air being expelled through the lower entrance. This process was first described by Thury (1861)

and the type of cave in which it occurs was referred to as "dynamic".

The third mechanism for cave ice accumulation, cold air trapping, is the most relevant to

our study. The model was first proposed by Thury (1861), where he defined such caves as

"static". In caves with one or more entrances at the same elevation and descending passages,

which is the case for the lava tubes in this study, cold air sinks when the air temperature outside is lower than that of the cave, pushing warm air out of the upper entrance. This cold air is "trapped" in the summer when warm, lighter air is unable to enter. During these months, a certain amount of ice melting does occur as the cave air temperature rises near the entrance as a result of direct sunlight shining on the ice or due to heat conduction through the bedrock. This rise in temperature is largely cancelled out however, as the melting process cools the cave air and helps maintain negative temperatures (Perşoiu & Onac, 2018).

2.4.2 Cave Ice as a Paleoclimate Archive

The first investigations into the use of cave ice in paleoclimatology focused on the relation of ice mass balance and temperature (Şerban, 1987; Racoviţă & Şerban, 1990; Ohata et al., 1994; Luetscher et al., 2005). Like the Antarctic and Greenland ice sheets, perennial cave ice stores a record of oxygen isotope ratios reflecting changes in climate. Isotope analysis, first examined by Şerban et al. (1967) and now a popular technique in cave ice paleoclimate reconstruction, has had mixed results. In one study by Yonge & MacDonald (1999), it was found that ice in the Canadian Great Divide exhibited isotope values exceeding that of local precipitation, with a decrease in $\delta^{18}O$ with cave air temperature increases. They attributed this to hoar ice deposition during warm seasons enriching the cave ice in the heavier isotopes.

Fórizs et al. (2004) also found higher isotope values in cave ice than in local precipitation from a cave in the Bihor Mountains, Romania. They attributed this heavy isotope enrichment to ice ablation and/or evaporation. Kern et al. (2004) report conflicting results with those of Yonge & MacDonald (1999), with a positive correlation between T_{air} and $\delta^{18}O$, when studying Focul Viu Ice Cave in the Bihor Mountains. One study of cave ice in Lecco (Italy) by Citterio et al. (2004) noticed that the isotopic values become more negative with depth.

18

2.4.3 Previous Studies on Cave Ice in New Mexico

In his M.S. Thesis, Dickfoss (1996) studied the chemical and physical composition of ice cores from La Marchantia and Candelaria Ice Caves (LIC and CIC) located in the central part of ELMA. His findings on the history of ice and its continued ablation in CIC were published a year later (Dickfoss et al., 1997), but without reporting any additional oxygen isotope data. The oxygen isotope values from the CIC and LIC ice cores in his Thesis were compared to those of local precipitation (Fig. 8) collected at the Cerro Montoso Weather Station (1980 m and 1840 m of elevation, respectively), and later reported by Pendall (1997). The station is located at 34°21'N, 106°31'W, approximately 160 km southeast of El Malpais National Monument. These results are relevant to our study and will be compared with our own proxy values in the Discussion Chapter.
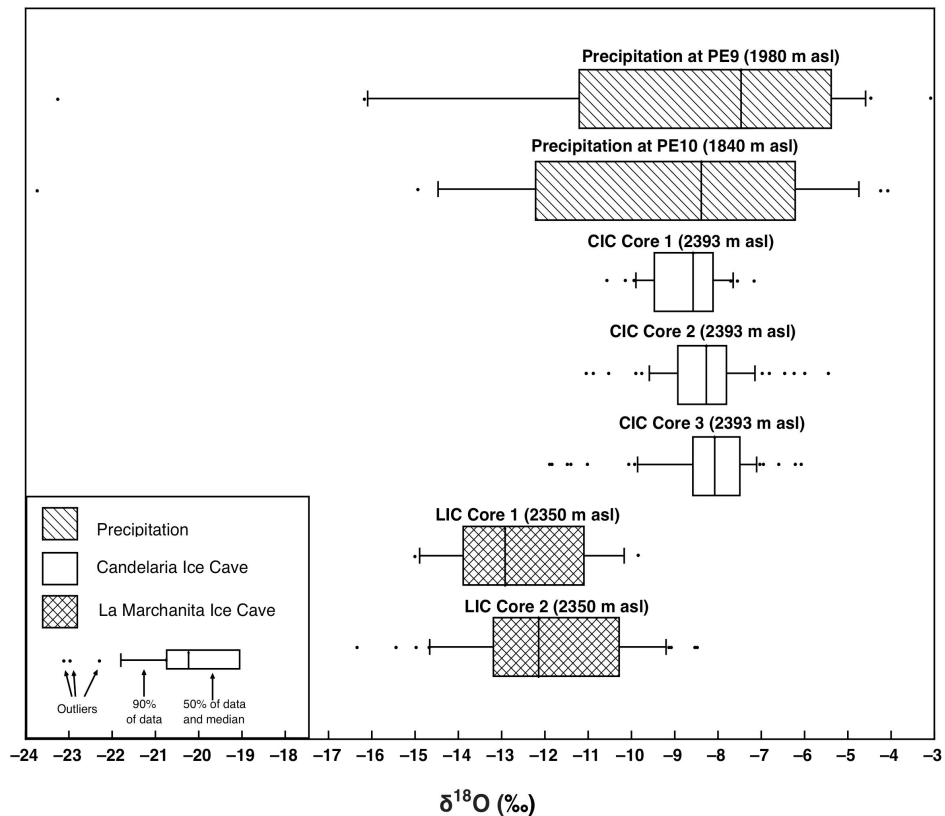
Figure 8: $\delta^{18}O$ box plot comparison of isotopes in LIC and CIC ice cores and precipitation from the Cerro Montoso Weather Station (modified after Dickfoss, 1996).

19

δ^{18}O values from the CIC ice cores in El Moro range from -5.65 to -11.69‰. Cores from

LIC contained δ^{18}O values between -8.58 and -15.49‰. The meteoric δ^{18}O values measured in

the precipitation collected by Pendall (1997) range between -17 and -5‰, with the majority

falling between -12 and -5.5‰. It is important to note that the ice core oxygen isotopes are well

within the range of local meteoric values, indicating that they are very much representative of

those in local precipitation. The LMWL obtained for rainfall at Cerro Montoso is given by the

equation below:

$$\delta^2H = 8 \cdot \delta^{18}O + 13.5,$$

which has the same slope as the GMWL indicating a lack of evaporation during precipitation.

The higher d-excess may suggest a lower humidity at the moisture source.

2.5 Carbon and Nitrogen Stable Isotope Analysis in Paleoclimate

2.5.1 The Carbon Cycle

Carbon is present on our planet primarily in two large reservoirs: ocean and crust. The

ocean maintains equilibrium with atmospheric carbon through the incorporation and expulsion of

carbonate, bicarbonate, and carbonic acid (as a function of pH), and by absorption into plants via

photosynthesis (Fritz & Clark, 1997). In order for the land reservoir and the atmosphere to

maintain carbon equilibrium, an immense amount is absorbed into soil as organic carbon via

photosynthesis and decomposition (112 x 10^{15} grams/year), and is returned to the atmosphere via

the decomposition of plants and other organic matter in soil (Sharp, 2007). This large amount of

carbon flux has kept atmospheric concentrations of carbon in the form of CO_2 low and relatively

constant throughout time.

Anthropogenic activity since the industrial revolution has led to a large increase in

atmospheric CO_2 concentrations. It has been estimated that as of 2016, over 36 billion metric

tons of CO_2 is released into the atmosphere every year from the burning of fossil fuels (NOAA, 2017). This disruption in atmospheric and land/ocean CO_2 equilibrium has had a direct impact on global temperature increases for the past 150 years, leading to an increased rate in sea level rise, as well as more frequent droughts and fires in regions like the Southwest US (Walsh et al., 2014).

A side effect of the anthropogenic CO_2 released to the atmosphere is the so-called *^{13}C* ***Suess effect*** that is responsible for a change in the average global $\delta^{13}C$ in the atmosphere from 6.5‰ in preindustrial times (prior to AD 1850) to less than 8.0‰ today (Keeling et al., 1979). This is due to the fact that combustion of fossil fuel, which is strongly depleted in the stable isotope ^{13}C due to the preferential uptake of the lighter ^{12}C isotope during photosynthesis (Andres et al., 1996), results in a reduction of the $^{13}C/^{12}C$ ratio of atmospheric CO_2. Given this postindustrial isotopic shift, all $\delta^{13}C$ values needs to be corrected for the Suess effect (see Methods).

2.5.2 C₃, C₄, and CAM Photosynthetic Pathways and δ¹³C

There are three primary pathways in plant photosynthesis, C_3, C_4, and CAM. C_3 photosynthesis, which gets its name from the 3-carbon molecule produced during the reaction within leaves, is the oldest and most common pathway. C_3 plants such as trees and shrubs fix carbon directly from the air, but this process is heavily dependent on the atmospheric CO_2 concentrations. As a result of decreases in global atmospheric CO_2 concentrations millions of years ago, some plants modified their photosynthetic pathways to maximize CO_2 retention (Sage, 2004). These C_4 (4-carbon molecule) plants transfer the absorbed CO_2 to bundle sheath cells before the reaction occurs, where a lower oxygen content ensures higher efficiency in carbon

21

fixation (Hatch et al., 1966). The majority of C_4 plants are angiosperms, and thrive in the

relatively low CO_2 and higher temperature environments compared to C_3 plants.

CAM (crassulacean acid metabolism) plants have adapted to extremely arid environments

where stomata are must remain closed during the day to prevent water loss. Carbon dioxide in

these plants is instead absorbed through the stomata at night, and is converted to malate

molecules and stored until photosynthesis can begin in daylight (Ranson & Thomas, 1960).

Smith & Epstein (1971) demonstrated that each photosynthetic pathway produces a

characteristic range of $\delta^{13}C$ values. Further studies by O'Leary (1981) and Cerling et al. (1997)

show that the $\delta^{13}C$ values of C_3 plants range between ~ -24 to -32‰ (averages at -26.6 ± 2.3‰)

and for C_4 plants from ~ -10 to -16‰ (average -12.5 ± 1.1‰), with CAM plants typically

showing $\delta^{13}C$ values in between C_3 and C_4. Variations in $\delta^{13}C$ values within the C_3 or C_4

photosynthetic pathways are largely the result of alterations in plant light-use, CO_2 recycling in

the canopy, and water-use efficiency (WUE) (Lambers et al., 2008). Since WUE is primarily

dependent on CO_2 concentrations in the atmosphere and rainfall amounts, one can use $\delta^{13}C$

variations within C_3 and C_4 pathways as a proxy for different hydroclimate conditions (Silva &

Horwath, 2013; Forray et al., 2015).

2.5.3 $\delta^{13}C$ Fractionation in the Bat Food Web

After carbon dioxide is absorbed by plants through photosynthesis, depending which

pathway they use (C_3, C_4, or CAM), the $\delta^{13}C$ signature of plants is transferred into the chitin of

the insects that feed on them at the larva stage, hence reflecting their diet. Along the plant-

insect-bat-guano pathway, the carbon isotope fractionation is minimal (Marais et al., 1980;

Wurster et al., 2007; Onac et al., 2014). In fact, it has been demonstrated that insects maintain a

$\delta^{13}C$ ratio in their tissue enriched by an average of 2‰ relative to their diet (De Niro & Epstein,

1978). Further fractionation occurs in the production of insect-synthesized alkanes, resulting in a

1‰ depletion (Marais et al., 1980). By combining these two digits, we expect a total ^{13}C

enrichment in insects of 3‰ relative to the consumed plant. Carbon isotopes in these insect

alkanes are not expected to undergo further fractionation during the metabolic processes after

consumption by bats (Mitchell, 1972). Thus, the isotopic signature of insect remains is

transferred unaltered into the bulk guano.

The usefulness of δ^{13}C in guano-based paleoclimate studies resides in the fact that the

photosynthetic pathways that plants use all have identifiable ranges of δ^{13}C. Thus, changes from

C_3 to C_4 vegetation assemblages (especially prior to human presence) captured in the δ^{13}C values

of guano will help in deciphering the prevailing environmental conditions such as temperature

and precipitation at the time guano accumulated (Smith & Epstein, 1971; Ehleringer et al., 1997).

Vegetation in El Malpais consists of primarily mixed conifer areas mostly composed of

Pinus ponderosa (ponderosa pine), shrub/conifer areas, and grass/shrub land consisting of

multiple species of C_4 grasses (Bleakly, 1997). Because of the extensive foraging range of

Tadarida brasiliensis (~80 km), the insects consumed will have δ^{13}C signals that vary depending

on whether they foraged primarily over grassland (C_4) or conifer areas (C_3) (Davis et al., 1962).

The dietary preferences of the 3 primary species of insects consumed by *Tadarida brasiliensis*

must also be considered. During evening foraging times, this species primarily consumes

carabidae, most of which as larvae are opportunistic omnivores that have little dietary

preference, and *lygaeidae*, which have a tendency to feed on milk-weed seeds (Davies, 1959;

Ralph, 1976; Whitaker et al., 1996). *Lepidoptera,* which are preferentially consumed during pre-

dawn feeds, can consume leaves from a wide range of plants during larva stages (Whitaker et al.,

1996). Since no in-depth study of insect diet in El Malpais is available, it must be assumed that

the majority of the insects consumed by bats obtained their $\delta^{13}C$ and $\delta^{15}N$ signal from whatever

plants were most available in the foraging area.

2.5.4 $\delta^{15}N$ and the Nitrogen Cycle

Nitrogen accounts for 78% of the Earth's atmosphere and represents the main source for

plant usage (Vitousek et al., 1997). While much of the modern nitrogen content on land has an

anthropogenic origin, the primary source outside of human involvement can be found in biotic

fixation, accounting for 110 Tg yr^{-1} (Gruber & Galloway, 2008). Anthropogenic activities such

as fossil fuel burning and agriculture, on the other hand, are responsible for ~160 Tg y^{-1}, while

approximately 98 Tg y^{-1} is retained on land or converted to N_2 through denitrification (Galloway

et al., 2004; Gruber & Galloway, 2008). A full depiction of the Nitrogen cycle in both land and

ocean environments can be further examined in Figure 9.
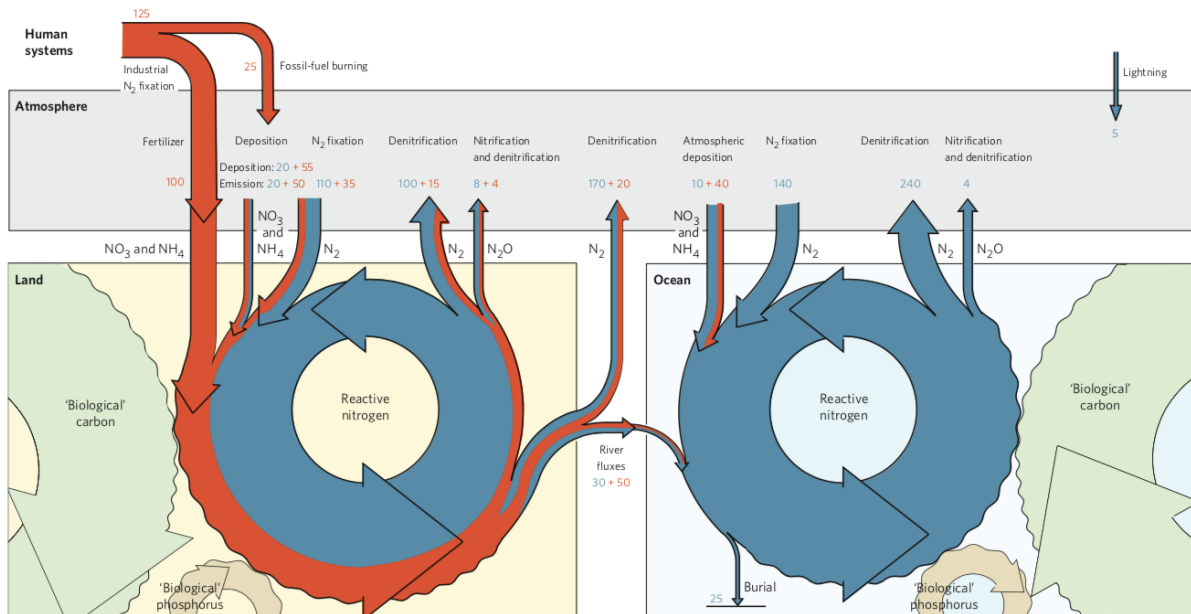
Figure 9: An illustration of the nitrogen cycle in both terrestrial (**left**), and ocean (**right**) environments. Sources include man-made (orange) and natural (blue); values are given in Tg y^{-1} (from Gruber & Galloway, 2008).

Nitrogen in guano has only recently been used in paleoclimate studies, primarily because of the relative complexity of the nitrogen cycle as well as the involvement of microbial processes in decomposition. The degree of fractionation in the nitrogen isotopes following deposition can be indicated by the C:N ratio and chemical composition of guano (Bird et al., 2007; Wurster et al., 2015). In a study by Robinson (2001), it was found that $\delta^{15}N$ could be used as an integrator for the Nitrogen cycle and therefore used as a record of the processes involved such as fractionation, nitrogen pool mixing, and nitrogen content percent variations. The $\delta^{15}N$ values can also be used to determine past anthropogenic activities such as use of fertilizer in agriculture, deforestation, and fires (Kendall et al., 2007). Multiple studies on nitrogen isotopes in vegetation and soil found that a relationship exists between $\delta^{15}N$ and precipitation, with decreases in $\delta^{15}N$ corresponding with wet periods and vice-versa (Austin & Vitousek, 1998; Handley et al., 1999; Robinson, 2001; Swap et al., 2004).

2.5.5 $\delta^{15}N$ Fractionation in Soil

There are multiple stages in the bat food cycle, each of which may cause nitrogen isotope fractionation. The source of nitrogen in this cycle is found in dissolved inorganic nitrogen (DIN) in soil, which has an isotope signature dependent on processes such as ammonification (fractionation is negligible), ammonia volatilization, nitrification, and denitrification (Table 1) (Högberg, 1997; Robinson, 2001; Tiunov, 2007). All of these transformations lead to a kinetic fractionation in which the heavier isotope is enriched (Högberg, 1997).

Table 1: Organic processes in soil causing ^{15}N enrichment (values are expressed in ‰; from Robinson, 2001).

Process	Reaction	Enrichment
Ammonification	Organic N → NH_4^+	~0–5
Nitrification	NH_4^+ → NO_2^- → NO_3^-	15–35
Denitrification	NO_3^- → NO_2^- → N_2O → N_2	28–32
Ammonia Volatilization	Urea → $NH_{3\ (gas)}$	40–60

2.5.6 $\delta^{15}N$ Fractionation in Plants

Certain fungi (*mycorrihizal* and *ectomycorrhizae*), which help roots with nitrogen uptake in a symbiotic relationship, have been found to fractionate nitrogen during the transfer process to roots, leaving a lower $\delta^{15}N$ value in them while increasing them in fungi (Högberg, 1997; Hobbie et al., 2000). After absorbing nitrogen (as ammonium and nitrate) from soil via their root systems (sometimes assisted by fungi) or from the atmosphere through fixation, metabolic processes within plants tend to cause further enrichment of the heavier isotope (Evans, 2001). These metabolic processes include nitrogen reallocation, nitrogen loss in specific organs, and multiple assimilations.

2.5.7 $\delta^{15}N$ Fractionation in Insects and Bats

As mentioned in previous sections, large scale changes in dominant vegetation type will be reflected by the isotopic signature of guano. For more recent guano accumulations, the variations of the $\delta^{15}N$ values will be largely dependent on the chosen foraging area and the specific diet for each bat species. Because the 80 km foraging range of *Tadarida brasiliensis* encompasses grassland, forest, and the Rio Grande, the $\delta^{15}N$ is likely to vary according to the forage location preferences of this particular species (Davis et al., 1962). As nitrogen moves along the bat food web, it becomes even further enriched in ^{15}N. This is due to the fact that after

the consumption of insects, much of the absorbed nitrogen is lost as ammonia in urea, with the lighter isotope preferentially converted and lost (Adams & Sterner, 2000; Kelly, 2000). As nitrogen makes its way up the trophic levels through larvae, insects, and finally to bats, $\delta^{15}N$ will increase by ~3‰ for each level (Kelly, 2000).

<center>

Chapter 3:

Methods

</center>

Note To Reader

All photos with visible individuals have permission granted for use in this thesis.

3.1 Sample Collection

3.1.1 Ice Coring Procedure

A Bosch hand held corer was used to recover the first 50 cm core from Cave 29. We employed a 100 cm long and 7.25 cm diameter Kovacs Mark 3 (COS-710-002) corer to collect samples from Cave 91 and the lower 50 cm of the Cave 29's ice deposits. We extracted a 100 cm core from Cave 91 (Fig. 10), which was then divided into 5 cm blocks, each of them crushed inside plastic bags before being transferred to plastic bottles. Two cores were recovered from the same location in Cave 29, 50 cm in 2017 (cut into 2 cm intervals) and 100 cm in 2018 (cut into 5 cm slabs due to lack of organic matter for use in dating) (Fig. 11). Since we used the same starting depth for both cores and they were taken within 10 cm of each other, we can combine them for use in analysis as one 100 cm core.

The cave settings in Cave 455 were unfavorable for vertical core extraction (narrow passage with low ceiling). Therefore, samples were taken horizontally along a vertical section (122 cm) using a Petzl ice screw at 2 cm intervals down the ice cliff (Fig. 12). Nitrile gloves were used for every step involving handling of the ice cores.

<center>28</center>

Figure 10: **Left:** Coring the ice deposit from the floor of Cave 91. **Right:** Image of the recovered ice core.

Figure 11: **Top and Bottom Left:** Test coring of the upper 50 cm in the Cave 29 ice block.

Top & Bottom Right: Coring the 1-m long ice core from Cave 29.

Figure 12: **Left:** The ice wall in Cave 455. **Right:** Recovering short, horizontal ice cores at 2-cm intervals using a Petzl ice screw on the ice wall of Cave 455.

3.1.2 Guano Coring Procedure

The guano pile in Bat Cave was cored using a meter-long Russian Peat Borer with a twist handle and extending rods (Fig. 13). This device's twisting motion is meant to prevent inter-layer mixing. Without a mechanical drill, extraction was more difficult and only a 70 cm core was recovered from a large guano mound accumulated along the main tube passage (Fig. 14).
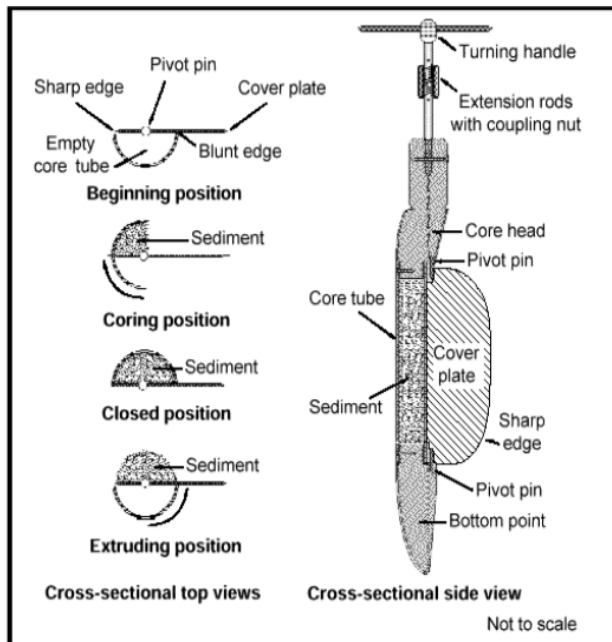
Figure 13: A sketch of the Russian Peat Corer used in recovering guano from Bat Cave (with permission from Aquatic Research Instruments 2018).

30

Figure 14: **Left:** A guano mound located in Bat Cave. **Right:** The guano core retrieved from Bat Cave showing some internal layering.

3.2 Isotope Analysis

3.2.1 δ^{18}O and δ^2H in Ice

Ice samples were melted at room temperature before being transferred to smaller glass bottles filled to the very top to prevent evaporation. They were then transported to the University of South Florida (USF), School of Geosciences, where the isotope analysis were performed on a Piccaro L2130-i Cavity Ringdown Spectroscope. About 0.8 mL of ice-melted water was filtered using 0.22 μm silicon disk filters before filling the 2 mL Piccaro vials.

All δ^{18}O and δ^2H values are reported in ‰ relative to VSMOW. Two in-house standards: USFW1 (δ^2H = -136.09 ± 0.1‰, δ^{18}O = -17.62 ± 0.08‰) and USFW2 (δ^2H = -0.01 ± 0.12‰, δ^{18}O = 2.37 ± 0.07‰) were calibrated against VSMOW2 and SLAP2. Since the standards used in analysis displayed deviations in reproducibility of δ^{18}O < 0.06‰ and δ^2H < 0.2‰, both within and across separate Picarro runs, drift correction was deemed unnecessary.

3.2.2 $\delta^{13}C$ and $\delta^{15}N$ Isotope Analysis

Guano samples were homogenized using a Crescent Wig-L-Bug LP-602E and an agate

vial and agate grinding ball (International Crystal Labs). We then weight out two milligrams of

each sample and sealed them in tin capsules. A Costech ECS4010 Elemental Analyzer (Costech

Analytical Technologies ECS) coupled to a Delta V Advantage Isotope Ratio Mass Spectrometer

(ThermoFisher Scientific) in the Isotope Lab of the School of Geosciences (USF) was used to

analyze the samples for carbon and nitrogen isotopes.

Three standards were used during bulk guano isotope analysis: B2155, a protein standard

(Elemental Microanalysis Ltd.), glutamic acid (GLU, internal standard), and USGS-40, the

official USGS L-glutamic acid standard. The in-house glutamic acid standard (GLU) has

measured values of $\delta^{15}N$ = -16.5‰ and $\delta^{13}C$ = -6.28‰. The precision of analysis was estimated

based on replicate standards in each run ($\delta^{15}N$: 0.18‰; $\delta^{13}C$: 0.04‰). Due to post-industrial

revolution increases in atmospheric CO_2 concentrations, $\delta^{13}C$ values have been adjusted using

the Suess Correction, which is implemented by subtracting the Suess effect from our time series

model, and is based on the global $^{13}CO_2$ record (Keeling et al., 1979).

3.3 Radiocarbon Dating and Age-Depth Modeling

3.3.1 Principles of Radiocarbon Dating

The radiocarbon dating method is based on the fact that the radiogenic carbon isotope

(^{14}C) is constantly being created when cosmic rays interact with nitrogen in the upper

atmosphere. This unstable isotope is eventually oxidized into $^{14}CO_2$, which then enters the

global carbon cycle and is assimilated by animals and plants throughout their lifetimes. We

expect carbon in the tissue of living organisms to be in equilibrium with atmospheric

radiocarbon, and that when organisms die this isotope will begin to decay to the stable ^{14}N

isotope. We can therefore use the half-life of ^{14}C (5,730±40 years) to precisely determine the age, assuming the organism in question was in a closed system after death where it no longer interacted with atmospheric radiocarbon and no amount of the daughter isotope was initially present (Libby, 1955; Taylor, 1997). As ^{14}C travels through the bat food web through plants and insects, it is expected to maintain equilibrium with atmospheric radiocarbon until after deposition in guano, when it begins to decay (Taylor, 1997). Radiocarbon in charcoal pieces and organic sediments found in the three ice cores should likewise allow for the precise age determination of these respective organic materials.

3.3.2 Sample Collection/Preparation for Radiocarbon Dating

Large charcoal samples from the upper part of the Cave 29 core, specifically at 0-2, 15-20, and 53-55 cm depths, were recovered from the ice-melted water and sent to the National Institute for Physics and Nuclear Engineering in Romania, where they were radiocarbon dated using a 1 MV Tandetron accelerator mass spectrometer (AMS).

Samples from the Cave 455 ice core were completely lacking in sediment and were therefore not sent for radiocarbon dating. For Cave 91, as well as for the lower part of Cave 29 ice cores, some sediment with possible organic content was noticed. Therefore, we used silicate filters and a vacuum pump to extract any organic and other sediments available in key samples throughout the ice cores from these caves (Fig 15). Organic and/or inorganic material was extracted from samples at depths of 5-10, 25-30, 70-75, and 90-95 cm from the Cave 29 core. Lack of visual evidences for charcoal in the Cave 91 ice core led us to sample only the top and bottom of the core (5-10 and 95-100 cm) for radiocarbon dating.

Figure 15: Sediment filtered from melted ice cores to be sent for radiocarbon dating.

Guano samples BC-1 (64-66 cm), BC-3 (60-62 cm), BC-9 (48-50 cm), BC-11 (44-46 cm), BC-22 (22-24 cm), and BC-33 (0-2 cm) were homogenized using a Crescent Wig-L-Bug LP-602E and sent to the National Institute for Physics and Nuclear Engineering in Romania for radiocarbon dating.

3.3.3 Age Depth Modeling

Because the atmospheric ^{14}C concentration varies through time, and because nuclear testing in the 1950s dramatically altered these concentrations, calibration techniques using U-series dated carbonates and tree rings with known ages must be employed. Age-depth models were created using the Clam 2.2 code (Blaauw, 2010) run under R (version 3.01), an open-source statistical software (R Development Core Team, 2013). Clam code requires ages to be calibrated using pre- or post-bomb atmospheric conditions. Since we obtained ages both older and younger than 1950, post-bomb results were calibrated with CaliBomb (Reimer & Reimer, 2009) using the IntCal13 and the Northern Hemisphere Zone 2 post-bomb datasets, respectively (Reimer et al.,

2013). The pre-bomb sample was calibrated directly through R (version 3.01) with Clam 2.2 code.

As the Clam-generated age-depth model contains multiple sections within the same year, a method had to be designed to find the associated months for these samples. Based on the fact that we expect guano accumulation to occur between April and September, the periods in which the bachelor/maternity colony is active, we created an equation to precisely obtain the months within this time period:

$$(ID - Y) * N + S = M,$$

where ID is the interpolated date rounded to two decimal places, Y is the year, N is the number of months for which we expect guano to accumulate, and S equals the month in which the interval starts (e.g., January = 1), in our case being April when accumulation begins. Once a month (M) was obtained, this value was then converted back to a final age (FA) rounded to two decimals using the following equation:

$$(M - S)/12 + Y = FA,$$

so that the age could still be plotted with proper monthly spacing, S in this case being 1 since we are converting back to a 12-month interval.

Chapter 4:

Results

4.1 δ¹⁸O Values for Cave 91 and 455

The $\delta^{18}O$ values for the ice core in Cave 91 (see Appendix A, Table A.1) show a

decreasing trend for the first 25 cm (with the exception of the section between 15 and 20 cm) and

relatively stable values, averaging -9.3‰, throughout the rest of the core (Fig. 16A). The most

notable feature of the $\delta^{18}O$ results for Cave 455 (see Appendix A, Table A.2) is the large shift to

more negative values between 34 and 48 cm depth (Fig. 16B). $\delta^{18}O$ values throughout the core

oscillate between -11.4 and -7.6‰, except for the depth interval mentioned above where they are

as low as -12.5‰.
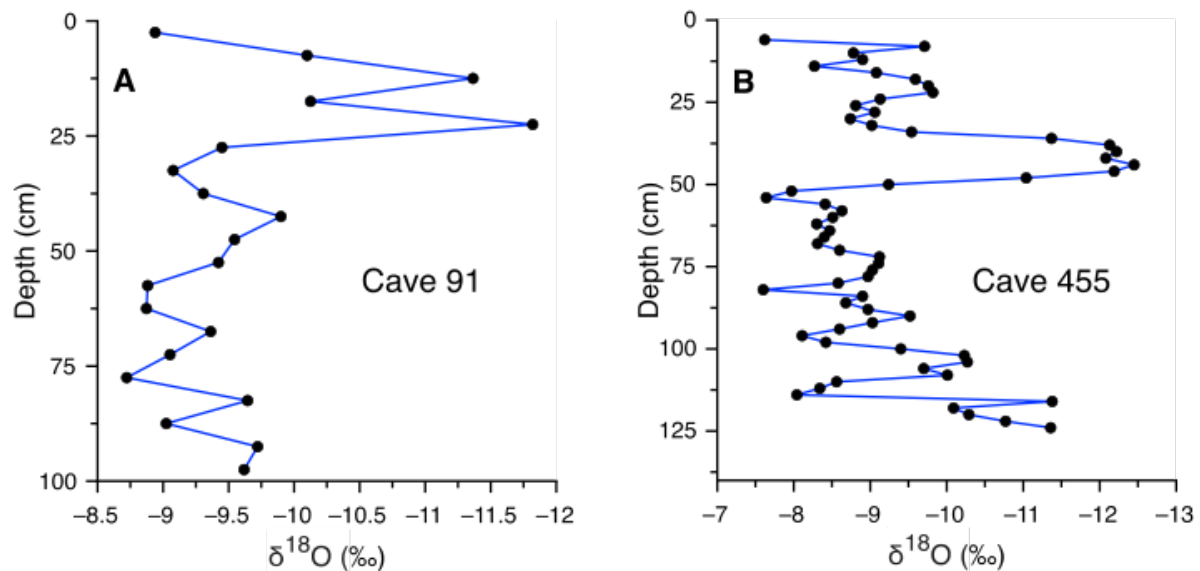
Figure 16: $\delta^{18}O$ vs depth plots for cave 91 (A) and 455 (B) ice cores.

4.2 Cave 29 δ^{18}O Time Series

The upper 57 cm of the ice core from Cave 29 was the only one with sufficient organic material (charcoal) available for dating. The radiocarbon ages obtained for the 4 samples sent for dating are listed in Table 2. One more age was obtained for the depth interval 5 to 10 cm, but it was out of chronological order and therefore discarded. The age depth model (Fig. 17) and δ^{18}O time series plot (Fig. 18) for this core are presented below (full results in Appendix A, Table A.3). A figure of δ^{18}O plotted with depth for the entire Cave 29 core is available in Appendix A (Fig. A.2).

Table 2: Radiocarbon ages and the calibrated years AD used to generate the age-depth model.

Sample depth (cm)	Radiocarbon age (yrs BP)	Calibrated 2σ age (cal AD)
1-2 cm	1105 ± 33	948 ± 13
15-20 cm	1148 ± 34	875 ±15
25-30 cm	1301 ± 22	693 ± 9
53-55 cm	1833 ± 74	192 ± 30
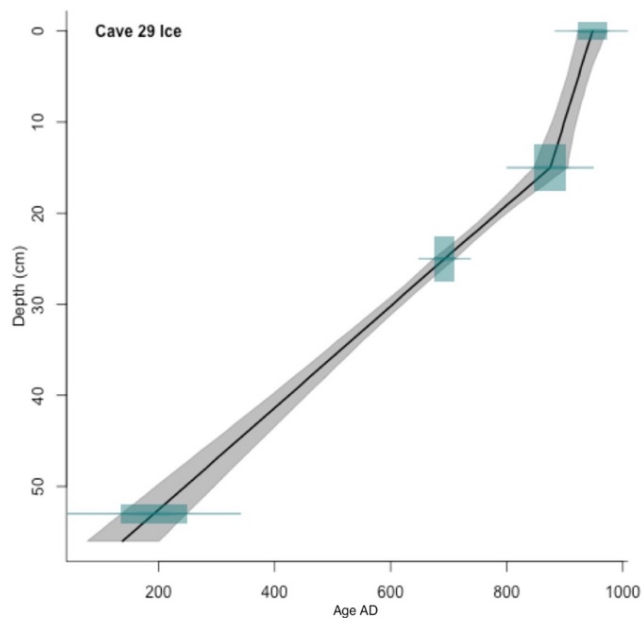
Figure 17: Age-depth model for the Cave 29 ice core.

37

The $\delta^{18}O$ time series, which assumes a continuous ice accumulation, reveals an overall decreasing trend until the second largest trough (-8.9‰) at ~AD 500 (Fig. 18). This is followed by a brief increase before plummeting to the lowest point at -9.3‰ (~AD 659). The remainder of the core displays an overall increasing trend with its highest peak of -6.9‰ at AD 919.
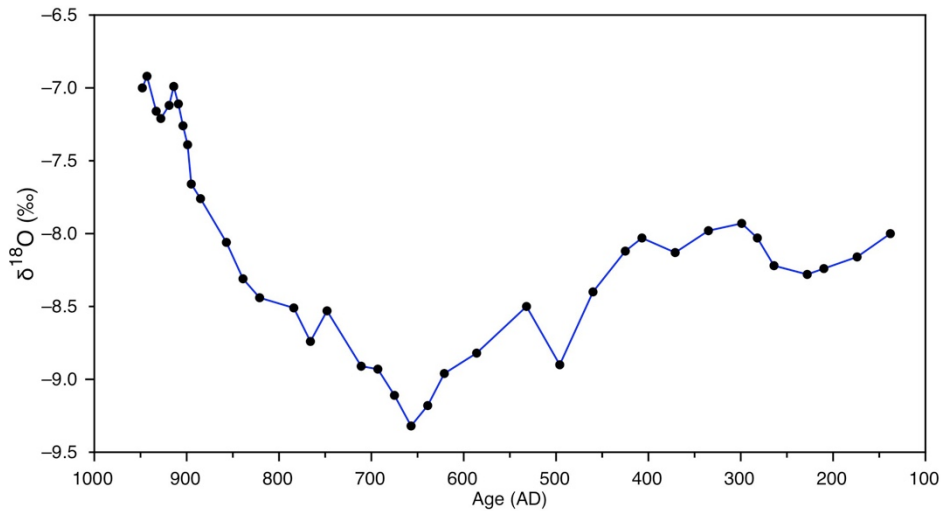
Figure 18: The ice $\delta^{18}O$ time series plot for Cave 29.

4.3 δ^2H Values and Local Meteoric Water Lines

δ^2H values across all cores have a minimum of -91.4‰ and a maximum of -28.7‰, with a mean of -59.1‰. LMWLs plotted for all three cores show good linear correlations with R^2 values > 0.90. The Cave 91 LMWL (Fig. 19A) displays a positive linear correlation between δ^2H and $\delta^{18}O$ values with an R^2 of 0.9889. The equation given by this relationship plots above the GMWL with a much higher d-excess of 17.5‰.

The LMWL plot obtained from Cave 29 (Fig. 19B) has an R^2 of 0.91317 and plots above the GMWL, but with a higher slope of 8.7. The d-excess obtained from this core approximates that of Cave 29 at 17.1. Cave 455 has a LMWL (Fig. 19C) that bears the closest resemblance to the GMWL with a slope of 8 and a d-excess of 9, with a good linear relationship defined by

R^2=0.98142. D-excess values plotted with depth for all 3 caves can be found in Appendix A, Figure A.1.
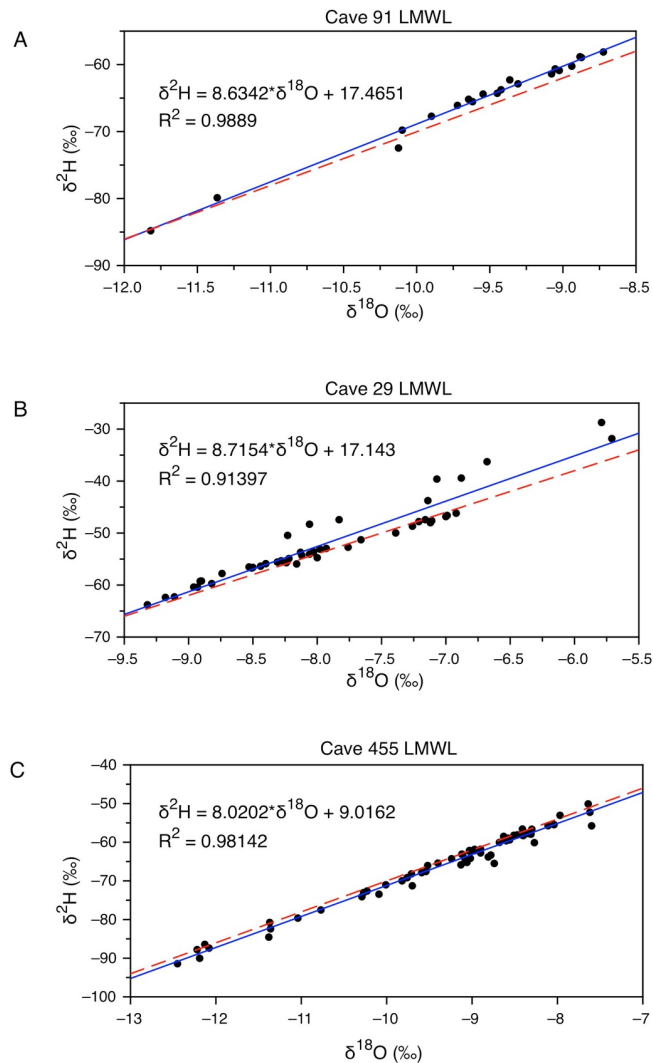
Figure 19: The Local Meteoric Water Line for cave 91 (A), 29 (B), and 455 (C) ice cores (blue line) plotted against the GMWL (red dashed line).

4.4 Guano Core Description, Carbon/Nitrogen % Content, and Age-Depth Model

The guano core exhibits varying sections of dark/light gray banding, with the lightest occurring between 21 to 28 and 34 to 42 cm in depth. The upper section is primarily composed of loosely bound guano pellets, while the lower part is noticeably darker and more compact. Based on three preliminary radiocarbon ages, it appeared that the guano accumulation between

the surface and a depth of 44 cm was much faster than in the lower part of the core. Therefore, we selected more samples from the lower part of the core to be sent for dating (Table 3).

Table 3. AMS ^{14}C measurements on guano samples and the calibrated years AD.

Sample depth (cm)	Radiocarbon age (yrs BP)	Calibrated 2σ age (cal AD)
0-2	-549 ± 27	2005
22-24	-592 ± 20	2003.5
34-36	-777 ± 28	1998
44-46	-276 ± 28	1956.5
48-50	-265 ± 21	1956
60-62	-321 ± 21	1955.5
62-64	337 ± 25	1584
64-66	321 ± 30	1564

The additional ages revealed a long hiatus between the lowest section of the core (AD 1584) and the rest, likely due to guano mining activities in the late 1800's and early 1900's. Ages for the upper 60 cm of the core cover the time interval between AD 1955 and 2006. The accumulation rate is noticeably faster between AD 1955 and 1957 (~9 cm/yr), where after it slows dramatically (~0.33 cm/yr) and increases again from AD 1998 to 2006 (~2.12 cm/yr). The age-depth model was generated by linear interpolation of these results using Clam code (Blaauw, 2010) is presented in Figure 20.
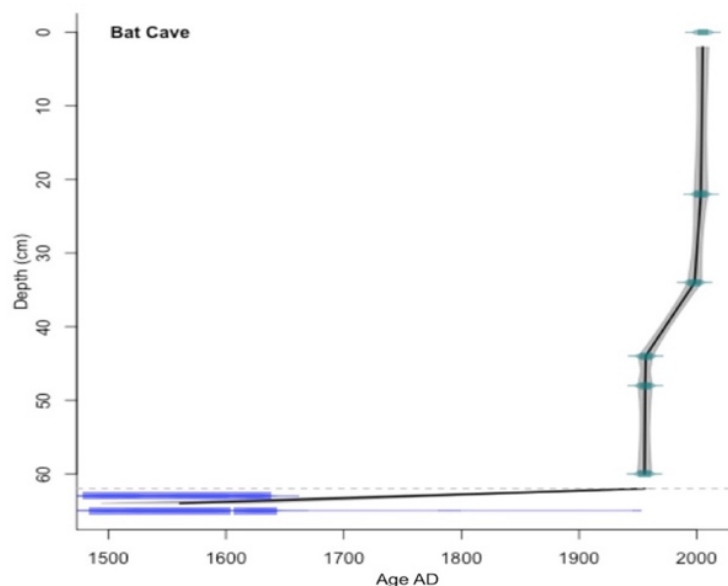
Figure 20: The Bat Cave guano age-depth model.

The % content of carbon and nitrogen, and C:N ratio are displayed in Figure 21. %N values remain relatively high and range between 11.6 to 16%. The %C values also maintain a relative stability and oscillate from 37.3 to 45.5%. The C:N ratio throughout the core never exceeds 3.5.
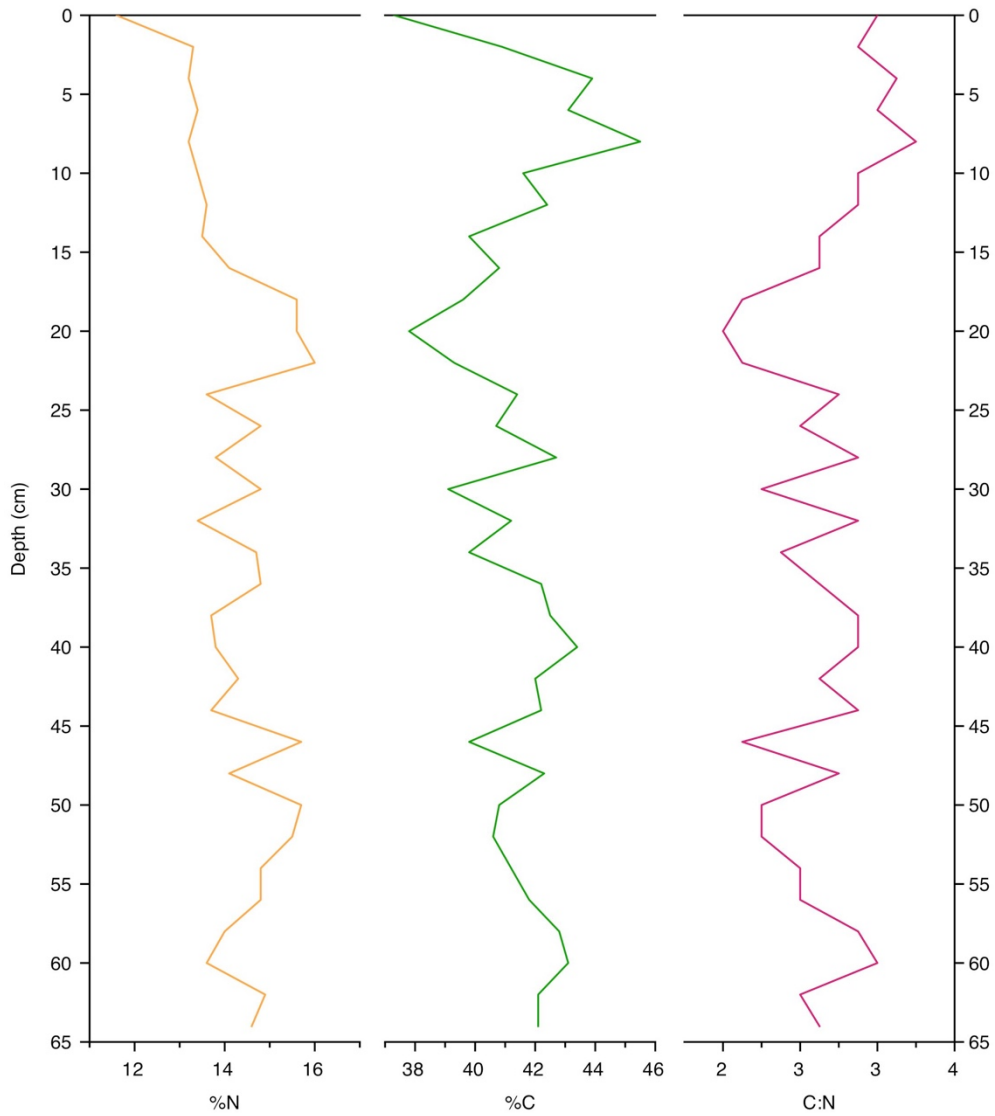
Figure 21: A comparison of %N, %C, and C:N in Bat Cave guano.

4.5 Bat Cave Guano δ¹³C Time-Series

The $\delta^{13}C$ time-series plot obtained from Bat Cave guano core is shown in Figure 22A

(full results are listed in Table A.4, Appendix A). Values range between -18.05 and -11.64‰; an

increase in $\delta^{13}C$ values can be noticed between the two samples from the bottom part of the core

defining the time period between AD 1564 and 1584. To better visualize the intervals with high

accumulation rates, i.e., AD 1955-1957 and AD 1998-2006, respectively, two separate plots were

created (Fig. 22B and C). The plot of $\delta^{13}C$ and $\delta^{15}N$ values against depth is available in

Appendix A, Figure A.4.
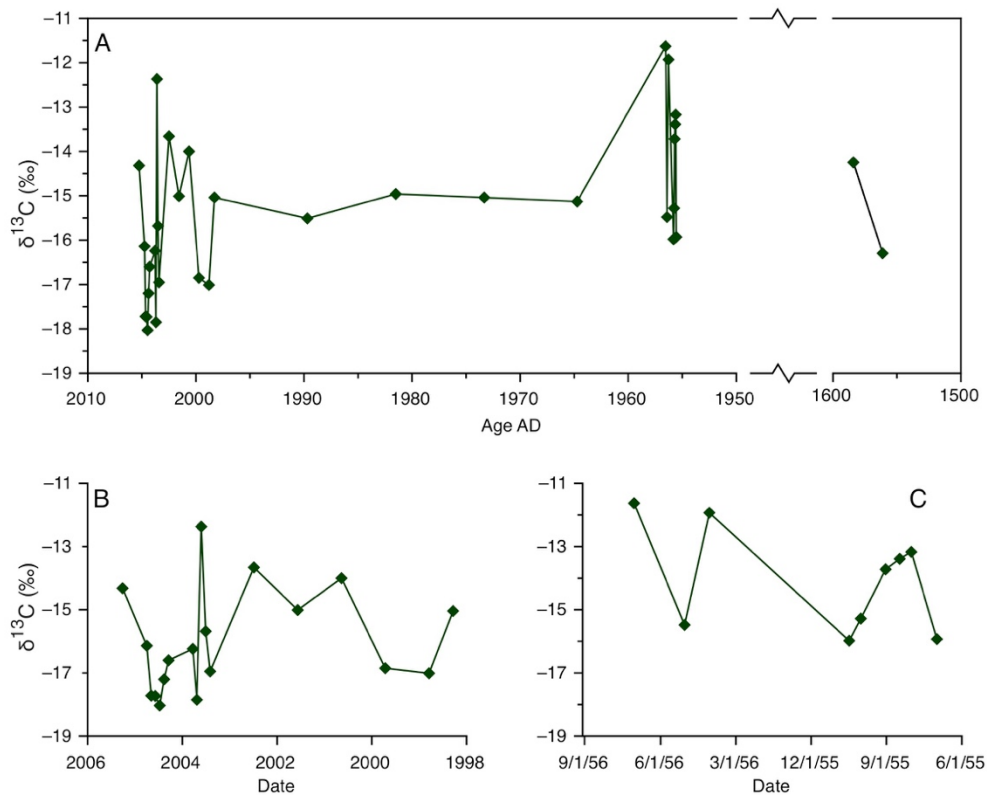
Figure 22: The Bat Cave guano $\delta^{13}C$ time-series (A), with close-up view for the intervals between 1998-2006

and 1955-1957 (B and C, respectively).

The average δ^{13}C value (-14.1‰) for the period from AD 1955 to 1957 is slightly higher than that of samples found at the top of the core, which is -16‰. The 1955 accumulation interval starts with increasing values in July and a decreasing trend in August. The most notable feature in AD 1956 is a trough (-15.5‰) in May. The δ^{13}C values of guano accumulation intervals between AD 1998 and 2006 show a maximum peak of -12.4‰ around August, 2003, and a minimum of -18‰ in June of 2004. The AD 2003 and 2004 periods have the highest resolution, covering full guano accumulation intervals, while the majority of values between 1998 and 2002 only include one value per year.

4.6 Guano δ^{15}N Time-Series

The δ^{15}N values range between 5.7 and 8.8‰ (Fig 23A). Because the accumulation rate was higher between AD 1955-1957 and AD 1998-2006, these intervals are plotted separately to better observe the isotopic fluctuations (Fig. 23B and C). δ^{15}N values of the samples at the bottom of the core corresponding to AD 1564 and 1584 are significantly higher than the majority of the upper core. After the hiatus, the δ^{15}N values are slightly below the previous ones and show an overall decreasing trend between AD 1955 and 1957, with the exception of a peak of 7.7‰ in May, 1956 (Fig. 23C). From 1957 to 1998 the general trend is an increasing one with a small trough in 1974. Values from AD 1998 to 2002 maintain a decreasing trend with a large peak of 8.2‰ in July, 2001. AD 2003 to 2004 values cover two full accumulation intervals with 2003 displaying a noticeable 2‰ increase while values in 2004 oscillate between 7 and 8.5‰.

Figure 23: The Bat Cave guano δ^{15}N time-series (A), with the intervals between 1998-2006 and 1955-1957 enlarged in panels B and C, respectively.
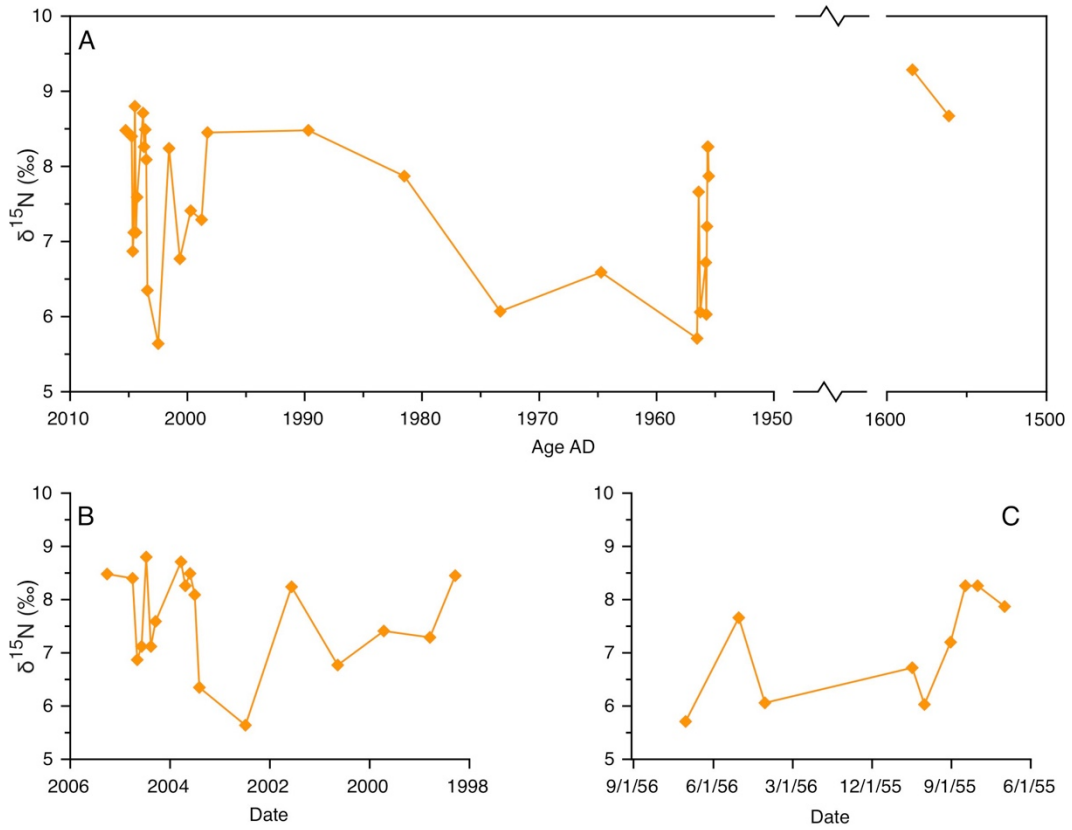
Chapter 5:

Discussion

5.1 Interpreting $\delta^{18}O$ Values in Ice Cores

5.1.1 Isotopic variations in Cave 91 and 455 Ice Cores

Due to the lack of organic sediment available for radiocarbon dating in the Cave 91 and

Cave 455 ice cores, it was impossible to create time series plots and make proper comparison

with other proxy records to further discuss the causes for the isotopic variations. That being said,

a certain amount of important information can still be derived from analyzing the amount of $\delta^{18}O$

fractionation within each of the cores. Studying the meteoric water lines and d-excess of these

cores can also reveal much about past moisture source and local climate conditions (Fig. 19 and

Fig. A1, respectively).

Cave 455 $\delta^{18}O$ values decrease as much as ~5‰ between 50 and 30 cm depth, whereas

Cave 91 values oscillate as much as 3.5‰ in the upper 30 cm (see Fig. 16). Using the Johnsen et

al. (1989) equation describing the relationship between local surface temperature and $\delta^{18}O$ values

in Greenland ice cores: $\delta^{18}O = 0.67T - 13$‰, we see that a 5‰ (from -12.5 to -7.6‰) change

would reflect a proportional ~7°C change in local surface temperature. It should be noted that an

equation relating temperature and $\delta^{18}O$ in ice from Greenland may not fully apply to the cave ice

in New Mexico, as it forms under very different climate conditions. Nevertheless, it at least

gives us an idea of how oxygen isotopes in ELMA precipitation may be responding to local and

regional temperature changes. Since it is unlikely that such a drastic temperature change (7°C)

could occur over a short interval, it is possible that other factors such as more Pacific-derived

precipitation (more negative $\delta^{18}O$) decreased values in the core. Melting of the upper layer of the Cave 455 ice block from contact with warm water in the summer may also have led to decreases in $\delta^{18}O$ values. The 3.5‰ oscillation in the Cave 91 core would have reflected local temperature changes up to 3.5°C. This increase in temperature is also high considering it only spans a 30 cm depth interval, and likely reflects the same moisture source changes we see in Cave 455.

The LMWL from Cave 455 has a slope that nearly matches that of the GMWL (Fig. 19). As discussed in section 2.3.2, variations in LMWL slope indicate evaporative processes during precipitation (Rozanski et al., 1993). Therefore, we can assume that the ice in Cave 455 was subject to little or no evaporation during precipitation in El Malpais. The d-excess value of 9.01 is slightly lower than the GMWL, suggesting faintly higher relative humidity at the moisture source compared to that of nearby land.

The LMWL derived from the Cave 91 ice core is defined by the equation $\delta^2H = 8.6*\delta^{18}O + 17.5$. The slightly higher slope relative to the GMWL signifies a small amount of evaporation during rainfall. A large d-excess of 17.5 infers a substantially lower relative humidity at moisture source. The Cave 455 LMWL shows a clustering of $\delta^{18}O$ values between -10.5 and -7.5‰, this is slightly higher than the concentration of values we see in Cave 29 (-10.3 to -8.5‰) and could indicate a higher frequency of summer precipitation in Cave 455 ice. Alternatively, the discrepancy between clustering in both LMWLs could suggests precipitation from a single moisture source but at varying temperatures, as seasonal changes alone at a single source can alter $\delta^{18}O$ values up to 6‰ (IAEA, 2010). If temperature is the primary cause for $\delta^{18}O$ variations in El Malpais, however, this would suggest a lower temperature (T) coefficient than the one found in the Johnsen et al. (1989) equation.

46

The clustering of both $\delta^{18}O$ and d-excess values in both caves may suggest a discontinuous accumulation of ice (see Figure A.1). This could mean that extreme precipitation events occurring in short intervals contributed to more accumulation, followed by periods of little or no precipitation/ice accumulation. Further study of accumulation rates based on a higher resolution chronology would allow to better understand the ice deposition. Furthermore, a mass balance that relates amount of precipitation and ice could be an important research goal for future studies.

5.1.2 Human Activity in Cave 29

Fragments of indented, corrugated pottery inside Cave 29 were identified as Cibola Grayware (Fig. 24) (Baumann, pers. comm., 2018). This type of ceramic is characteristic of the Ancestral Puebloan, from which the Acoma and Zuni peoples of El Malpais descend, and dates back to AD 800 to 1300. The section of Cave 29 where the ice block is located contains large charcoal mounds. It is likely that Native Americans had used fires inside the cave to melt ice for drinking water during periods of drought. This could explain why the top of our core was dated at AD 948, as the missing ice above could have been melted for drinking.

Figure 24: **Left:** Cibola Grayware fragment found on top of the Cave 29 ice block. **Right:** A large charcoal mound next to the Cave 29 ice block.

Several pits can be found between the cave entrance and the ice block. It is possible that they were dug to collect and store melted ice water to facilitate its usage. Another possible explanation for their presence would be that early settlers in the 1800's prospected the lava tube in search of precious metals. In support of this hypothesis comes traces of a mined section in the back of the cave, where miners used hammer and chisel. In addition, the upper part of a wooden ladder coming out of one of these pits (now an ice pond) suggests the miners dug rather deep exploration ditches.

5.1.3 The Cave 29 Ice δ^{18}O Record and Major Climate Events

The majority of local precipitation δ^{18}O values collected by Pendall (1997) fell between -17 and -5‰ (a 12‰ amplitude). While our values are within this range, they only vary up to 2.5‰ in the Cave 29 ice core. In his study on Candelaria Ice Cave in El Malpais, Dickfoss

(1996) found $\delta^{18}O$ in ice ranged between -11.7 and -5.7‰ (a 6‰ amplitude). He attributed this discrepancy between precipitation and ice $\delta^{18}O$ to three major causes, two of which are applicable to our study. First, because snow accumulates throughout the winter and enter the cave after melting, the $\delta^{18}O$ values for these months mix together and will produce an isotopic signal that represents an average of the entire season. Second, a small degree of melting due to rainfall-derived water percolating in the cave during warm seasons is responsible for mixing ^{18}O-enriched summer and ^{18}O-depleted winter precipitation. See Appendix A, Figure A.3 for a comparison of ice core $\delta^{18}O$ values from this thesis with the Dickfoss (1996) ice and Pendall (1997) precipitation values.

The upper 55 cm of the Cave 29 ice core spans the period between AD 138 and 948. The following analysis assumes a continuous ice accumulation between ages obtained from radiocarbon dating, but it is important to note that the clustering of $\delta^{18}O$ values could suggest a majority of accumulation happening during heavy rainfall events (See Figure A.1). The accumulation rate between AD 138 and 693 (0.05 cm/yr) is almost twice as fast as the period from AD 693 to 875 (0.027 cm/yr). After AD 875, accumulation speeds up dramatically to 0.18 cm/yr. The rates of accumulation for the entire core, however, are substantially lower than that of the CIC core studied by Dickfoss (1996), which reaches 3.1 cm/yr. This is likely due to the fact that ice in CIC accumulates next to one end of the collapsed lava tube ceiling, making possible for large amounts of rain and snow buildup to occur over a relatively shorter period of time, due to the proximity to the entrance.

There are three important climate events that occurred over the interval between AD 138 and 948: the Roman Warm Period (RWP: BC 250 - AD 450), Dark Ages Cold Period (DACP: AD 450 - 800), and the Medieval Warm Period (MWP: AD 800 - 1350). $\delta^{18}O$ values in our core

remain relatively constant throughout the end of the RWP, but plunge at ~AD 450 during the onset of the DACP. A steady increasing trend begins around AD 665, accelerating at ~AD 850, right after the beginning of the MWP. We found several other proxy records that span these climate periods for use in comparison (Fig. 25).

5.1.4 The Climatic Significance of $\delta^{18}O$ Fractionation in Ice: Temperature and Amount Effects

In understanding the relationship between our $\delta^{18}O$ values and temperature trends, we use the Ljungqvist (2010) multi-proxy reconstruction of Northern Hemisphere temperature (Fig 25B). While major peaks and troughs have little in common between this record and our own, the ice $\delta^{18}O$ values from Cave 29 do follow general Northern Hemisphere temperature trends, marking three distinct climate periods (RWP, DACP, and MWP). Ljungqvist's reconstruction marks the end of the RWP at AD 300, when Northern Hemisphere temperatures had decreased to a minimum average and stabilized. Other temperature reconstructions using lake sediments in northwest and southeast North America show a similar trend. Studies in Europe such as Hass (1996), or even earlier studies by Lamb (1982, 1985), identify AD 400 as the onset of the DACP. Our record however, shows a decreasing trend in $\delta^{18}O$ representing climate deterioration at the end of the RWP and transition into the DACP around AD 450. This is in closer agreement with the Follet et al. (2004) climate reconstruction which used changes in C3/C4 vegetation dominance as a proxy for temperature and precipitation in the Western Corn Belt and Great Plains, and noted a large transition to a colder climate at AD 450. A comparison of our record with the Trouet et al. (2013) North American temperature reconstruction based on pollen shows a similar trend with the lowest values in the DACP between AD 550 and 650, where after both records demonstrate an increase during the transition into the MWP.

50
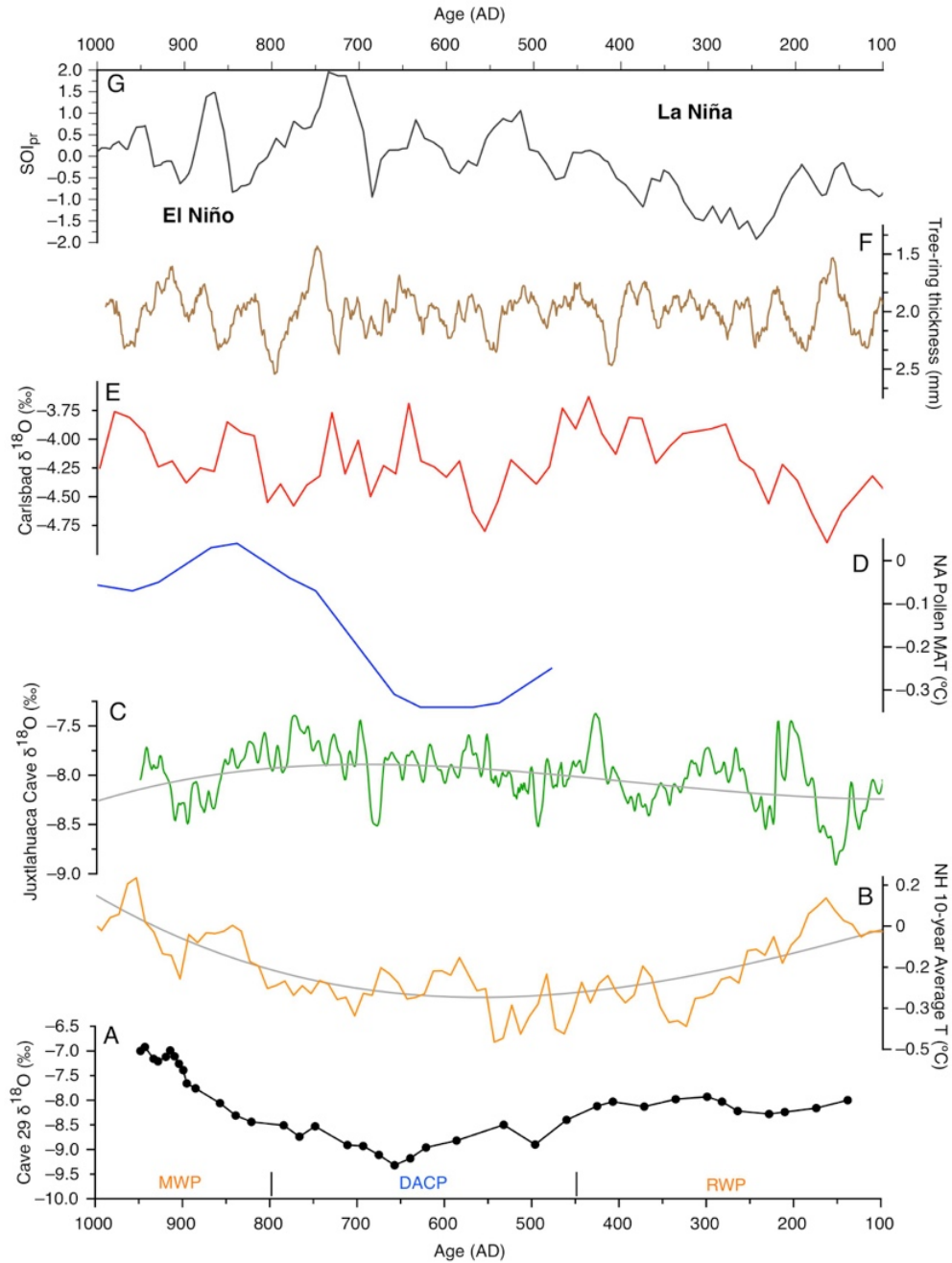
Figure 25: A comparison between the Cave 29 ice core δ^{18}O record (A), the Northern hemisphere multi-proxy temperature reconstruction (B; Ljungqvist, 2010), a δ^{18}O record from a speleothem in Juxtlahuaca Cave, Mexico (C; Lachniet et al., 2012), the North American 30 year resolution pollen temperature reconstruction by Trouet et al. (2003)(D), the Carlsbad, NM speleothem δ^{18}O record (E; Asmerom et al., 2007), the El Malpais 20-year average tree-ring thickness record (F; Grissino-Mayer, 1995), and the Southern Oscillation Index reconstruction by Yan et al. (2011) (G).

51

Fractionation in the Carlsbad Caverns speleothem $\delta^{18}O$ record documented by Asmerom et al. (2007) (Fig. 25C) was attributed mainly to changes in moisture source resulting from solar forcing, and in part to the amount effect. Therefore, we examine whether the amount effect affects our record as well. One way of addressing this is to make use of the dendrochronology study provided by Grissino-Mayer (1995) (Fig. 25F). When comparing the tree-ring thickness and the Carlsbad Caverns $\delta^{18}O$ values in speleothem (Fig. 25F and E), we noticed that increases in precipitation denoted by wider tree rings mostly correspond with decreases of $\delta^{18}O$ in speleothem calcite values. This is in agreement with the Asmerom et al. (2007) study that reported an amount effect on their speleothem, giving us an opportunity to evaluate the $\delta^{18}O$ values in the Cave 29 ice core against the record derived from the tree ring study conducted in ELMA by Grissino-Mayer (1995). The direct comparison of these two time-series show no similar trends or overlapping peaks (Fig. 25A and F), however, thus leading us to the conclusion that the amount effect has little to no impact on our ice core record.

5.1.5 Moisture Source Variation and ENSO

$\delta^{18}O$ values become more negative as the moisture travels from source to precipitation site due to the altitude and continental effects. This means that our range of values were closer to those of Gulf of Mexico summer precipitation (between -2 to -4‰) before undergoing such processes. Furthermore, in comparison with the trend line in the Lachniet et al. (2012) speleothem $\delta^{18}O$ record in Mexico (Fig. 25C), which was used as a proxy for NAMS strength, we see an anti-correlation with our values. This is due to the fact that unlike the $\delta^{18}O$ values in ice from El Malpais, the Juxtlahuaca speleothem values are primarily controlled by the amount affect due to the lower latitude of the cave (~18° N), decreasing in response to increases in

precipitation from the GoM. In our record we see an opposite response, as increased

precipitation from NAMS leads to more positive δ^{18}O values in ELMA precipitation. The

relative smoothness of our trends as compared to those in the speleothem record is likely due to a

difference in resolution.   Thus, we believe that ice in Cave 29 accumulated year-round, with the

majority building up during summer monsoon seasons (or ponding in the summer and freezing in

the autumn/winter), while a much smaller amount originates from winter precipitation from the

Pacific. Furthermore, variations in the frequency of precipitation from these two sources may

have the potential to cause shifts in our isotopic signal, and thus Winter precipitation from the

Pacific must be examined as well.

The frequency of winter precipitation received in the Southwest is largely modulated by

ENSO. During El Niño conditions, we see increased winter precipitation from the Pacific in the

Southwest and therefore expect a decrease in δ^{18}O. The opposite effect (a decrease in winter

precipitation) manifests during La Niña events. To investigate how changes in Winer

precipitation as modulated by ENSO may have impacted the isotopic values in ELMA, we have

provided a comparison of the δ^{18}O in the Cave 29 ice core to a reconstruction of the Southern

Oscillation Index (SOIpr) based on Pacific precipitation reconstructions using the Mg/Ca ratio in

foraminifera (Fig. 25G) (Yan et al., 2011). El Niño like conditions in this scale are inferred by

negative SOIpr values, while positive values denote a more La Niña-like state. Thus, we expect

to see a direct relationship between SOIpr and δ^{18}O anomalies in Southwest precipitation, with

positive SOIpr values indicating a decrease in winter Pacific precipitation (removing more

negative values while leaving higher values from the Gulf of Mexico unaffected), and therefore

increasing δ^{18}O values in cave ice. In comparing these records, however, we see little correlation

between ENSO conditions and δ^{18}O trends. This provides further evidence that the majority of

precipitation in ELMA for this period was from NAMS, which researchers as of yet have been unable to properly correlate to ENSO (Andrade & Sellers, 1988; Sheppard et al., 1999). The Cave 29 ice core $\delta^{18}O$ values thus primarily reflect local temperature variations, as well as changes in NAMS strength.

5.2 Possible Causes for Carbon and Nitrogen Stable Isotope Variations in Bat Cave Guano

While the resolution of our guano time series is not good enough to make solid conclusions based on comparisons with modern records, it is still worth examining to see if any obvious relationships present themselves. The range of $\delta^{13}C$ values in guano has been found in previous studies to be primarily influenced by the bat food web (changes in insect diet from C_4 and C_3 plants). Our relatively high values of $\delta^{13}C$ (-16 to -11.9‰) are the result of an insect diet consisting primarily of C_4 plants, which have their $\delta^{13}C$ range of -10 to -16‰ (O'Leary, 1981; Cerling et al., 1997). It is unlikely that such large fractionation (~4‰) in the $\delta^{13}C$ values of bulk guano could reflect WUE changes in our region. This becomes even more evident if considering a recent study on C_4 grass found that WUE causes only a ~1‰ difference in $\delta^{13}C$ between well-watered and water-limited plants (Ellsworth et al., in review). Our core covers a recent 50-year interval during which no dramatic changes in dominant vegetation type occurred. In addition, while El Malpais National Monument is largely conifer forest (C_3 plants), the Eastern edge of the monument is also covered with sparse grass, and several species of cacti can be found throughout the park (C_4 plants). The wide 80 km foraging range of *Tadarida brasiliensis* allows for the possibility of feeds outside of the park as well, inviting the likelihood of bats feeding in the large expanse of desert grassland to the north and south of the park. A vegetation study in ELMA by Bleakly (1997) found that the park contained four typical species of grasses, three of which use C_4 photosynthetic pathways. The relatively higher $\delta^{13}C$ values in our record can thus be

explained by a preference of *Tadarida brasiliensis* to forage over grasslands either within the park or outside it. Variations in this signal are most likely the result of bats changing their foraging area. However, because bats lack a well-developed ability to modulate body temperature, their foraging habits are highly dependent on environmental conditions (Herreid, 1959). Therefore, it is still worth investigating relationships between recent climate trends and our δ^{13}C record.

Since the δ^{15}N signal between the bottom and top of this 50-year interval exhibits only a 0.6‰ enrichment, and because samples throughout the core maintain a relatively stable, high %N content (11.6 to 16%), we therefore expect little to no fractionation due to processes such as denitrification or ammonia volatilization. This makes sense for our study area, as a lack of water availability and very low relative humidity in the cave would effectively arrest decomposition processes in guano (Mituzani et al., 1992). Cleary et al. (2017) concluded that δ^{15}N variations for guano in some Romanian caves are primarily controlled by winter precipitation. This is because while the insects in the bat food web are consumed in the spring/summer months, the δ^{15}N values in the plants they eat reflect soil nitrogen conditions before growth season in the late-fall and winter months. A study by Ma et al. (2012) characterize the specific relationship between δ^{15}N fractionation in plants and precipitation as -1.0 ± 0.1‰ per 100 mm of rain. The fact that precipitation for our time period never exceeds 40 mm, however, makes it unlikely that we would see much impact in δ^{15}N from rainfall. Other possible causes for variation in our δ^{15}N values include changes in *Tadarida brasiliensis* dietary habits. A preferential consumption of insect larva vs fully formed adults, for example, can cause a 3‰ difference in δ^{15}N (Kelly, 2000). The fact that *Tadarida brasiliensis* prefers carabidae beetles (which can be carnivorous) during evening feeds can also have an impact on δ^{15}N in guano (up to 3‰ due to an increase in

trophic level) (Davis et al., 1962; Kelly, 2000). Different C_4 plant species may also carry different $\delta^{15}N$ signals, but an in-depth study of the isotopic composition of various El Malpais vegetation types would be required to further analyze this topic.

Anthropogenic activities must also be considered when analyzing $\delta^{15}N$ trends in guano. While logging practices can affect nitrogen content in soil due to the removal of biomass and result in altering $\delta^{15}N$ values in plants in the bat food web, they are ultimately unrelated to our study period as logging practices in ELMA ended in 1942 (Glover and Hereford, 1986). Fires have the potential to alter $\delta^{15}N$ values in soil as well by increasing N removal by volatilization (McGrath et al., 2001). As such, we must also examine known fire records for the two intervals discussed below. Fires can also alter $\delta^{13}C$ values by impacting the bat foraging range or by altering the vegetation of the area affected, for example with C_4 plants in the foraging range being destroyed and replaced by new C_3 plants.

5.2.1 $\delta^{13}C$ and $\delta^{15}N$ variations in bulk guano from Bat Cave from AD 1955-1957

Since the accumulation rate in our record is much faster for two specific periods (AD 1955-1957 and 1998-2006), we have focused our comparison on these two intervals. The reason for this variation in accumulation rate is most likely due to a change in colony distribution inside the cave, with decreases in accumulation occurring when less bats roost directly above the coring site. It could also indicate changes in food availability and implicitly the number of bats in the colony. We have included temperature and precipitation values from the closest available weather station at the Grants-Milan Municipal Airport, approximately 30 km north from El Malpais (NOAA, 2018). The relationship between precipitation and $\delta^{13}C$ and $\delta^{15}N$ variation for the 1955-1957 interval (Fig. 26A and B) is only notable in 1956, when both records show a peak in May. It is unlikely that a direct correlation between these records and climate changes exists

on such short interval, however, considering $\delta^{15}N$ in the bat food web are expected to respond to precipitation changes from the previous cold season while $\delta^{13}C$ changes are much less delayed. The persisting arid conditions of this period (Fig. 25D), coupled with the lack of any correlation between our records and temperature (Fig. 26C), lend credence to the idea that isotopic variation in guano for this period resulted from dietary and foraging habit changes independent of environmental conditions.

Fires have the potential to decrease $\delta^{15}N$ values in soil by volatizing N and resulting in a closed nitrogen system (Davidson et al., 2007). Therefore, the incorporation of insects that fed on plants from areas affected by fire could potentially lead to the large variations in $\delta^{15}N$ we see in Bat Cave guano. Another effect that fire frequency and/or amplitude may have on our record for the AD 1955-1957 timescale is changes it could cause in *Tadarida brasiliensis* foraging range. The Grissino-Mayer (1995) study found that the tree ring records from Mesita Blanca and Hidden Kipuka areas of the park are the only ones to have displayed continuous fire frequency since the 1940's. If the *Tadarida brasiliensis* colony originally included the grasslands to the south of the park in their foraging area, fire activity in the aforementioned locations may have prevented them from feeding there. This would alter the $\delta^{13}C$ signal due to an inclusion of C_3 vegetation-fed insects and change $\delta^{15}N$ values by changing insect availability to include larva or carnivorous beetles in the bat diet (changing the trophic level).

Figure 26: A comparison between δ^{13}C (A) and δ^{15}N (B) with modern records with a single guano accumulation interval for the period AD 1955-1957. The scale for δ^{13}C has been reversed for clarity. Temperature (C) and precipitation (D) were recorded by the weather station at Milan-Grants Municipal Airport and are averaged from daily values.

5.2.2 Stable isotope variations in bulk guano from AD 1998-2006

The prevailing arid conditions (rainfall below 40 mm/month) for the period AD 1998-2006 (Fig. 27D and E), coupled with multiple oscillations in both δ^{13}C and δ^{15}N time-series (Fig. 27A and B) further demonstrates a lack of connection between precipitation and stable isotope variation for our record. The fact that δ^{13}C values for this period exceed the lower limit

for C[4] plants (-16‰) at times also lends evidence to the hypothesis of changes in foraging habits

to include areas dominated by C[3] plants.
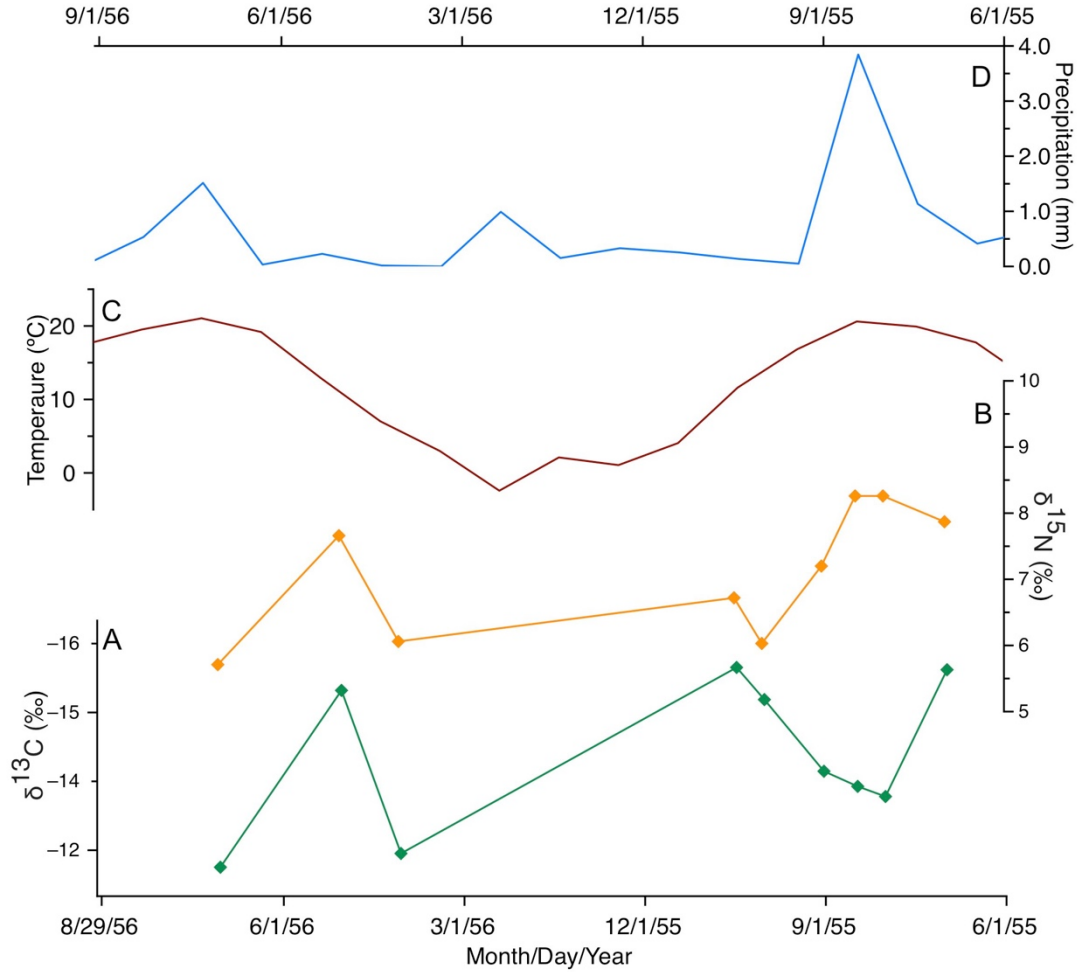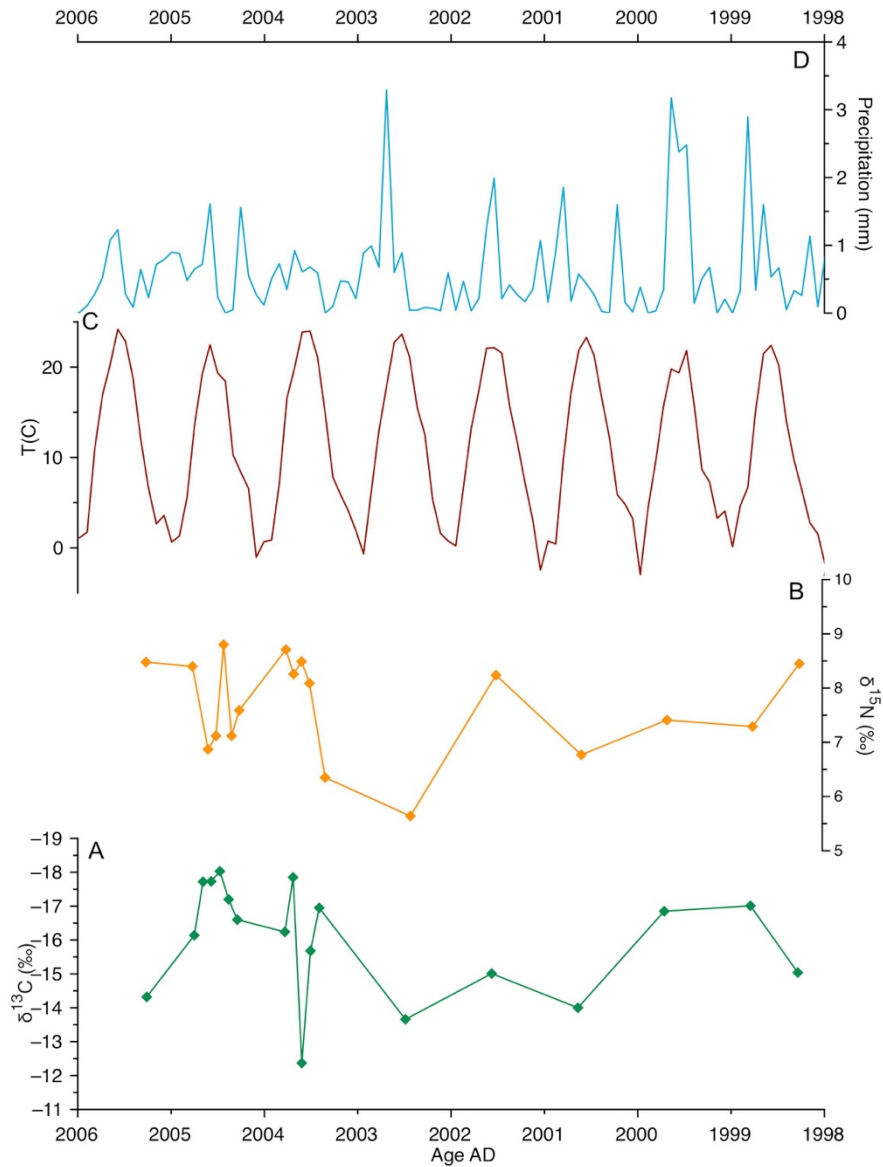

Figure 27: A comparison between $\delta^{13}C$ (A) and $\delta^{15}N$ (B) with modern records for three guano accumulation intervals during the period AD 1998-2006. The scale for $\delta^{13}C$ has been reversed to match the wet/dry scale. Temperature (C) and precipitation (D) were recorded by the weather station at Albuquerque International Airport and are averaged from daily values.

Trends in $\delta^{15}N$ for these periods bear little resemblance with temperature or precipitation variation, and are more likely the result of diet changes unrelated to climate. One event that may have led to the largest changes in $\delta^{15}N$ values for 2004 and 2005 was a fire that occurred near the Sandstone Bluffs on the northern edge of the park (Baumann, pers. comm., 2018). If insects feeding on plants in the Sandstone Bluffs were incorporated into the bat foraging range, they could have caused the large variations we see in $\delta^{15}N$ values for AD 2004 and 2005 (to include higher values from insects consumed in this area). The fire could have potentially restricted bat movement to the northern grasslands and resulted in increased the amount of C_3 vegetation type closer to the cave into the bat foraging range. This would then lead to the large decrease in $\delta^{13}C$ values seen in late 2003. This change in foraging area would have caused variations in insect diversity and availability that in turn would alter the $\delta^{15}N$ signal as well.

Chapter 6:

Conclusions

Stable isotope analysis of the three cores recovered from ice deposits hosted in lava tubes in El Malpais National Monument reveal a relationship between temperature and NAMS strength variations with $\delta^{18}O$ trends in ice. While the Cave 91 and 455 ice cores did not contain enough organic sediment to extract radiocarbon dates, the upper 55 cm of the Cave 29 core produced ages spanning the interval between AD 137 and 948. $\delta^{18}O$ trends in this core reflect changes in both North American temperature reconstructed from pollen (Trouet et al., 2013), and large-scale Northern Hemisphere temperature as found in the Ljungqvist (2010) study, decreasing after the transition from the RWP to the DACP, and increasing rapidly at the onset of the MWP. A correlation also exists between the Cave 29 $\delta^{18}O$ values and variations in NAMS strength as reflected in the Lachniet et al. (2012) Mexico speleothem record, with $\delta^{18}O$ in our core increasing when ELMA receives more frequent precipitation from NAMS.

Due to the mining activities by early settlers, our guano core from Bat Cave included a long hiatus near the bottom of the core at AD 1584, leaving us with a short, 50-year interval of accumulation between AD 1955 and 2006. The periods between AD 1955-1957 and AD 1998-2006 showed the fastest accumulation of guano and therefore had a higher resolution of $\delta^{13}C$ and $\delta^{15}N$ data points. As such, these periods were magnified for comparison with modern records. Our values (-16 to -11.9‰) fall within the range of C_4 plants, and are likely the result of *Tadarida brasiliensis* foraging in the C_4 grasslands to the north or/and south of ELMA. The large range of $\delta^{13}C$ values (~5‰) despite the overall lack of precipitation for this interval infers

that $\delta^{13}C$ variations in this record are primarily related with the foraging habits of *Tadarida brasiliensis*.

$\delta^{15}N$ values are also likely reflective of dietary changes largely independent of climate. While some fire activity was present for our interval, these events were few and far between and did not occur in the grasslands. It is possible that natural fires had an effect on $\delta^{15}N$ values, if the bat foraging range sometimes included insects that had consumed vegetation from areas that previously experienced such phenomena. They may also have altered the bat foraging area and affected insect availability, forcing bats to include carnivorous beetles or larva in their diet, which could potentially alter the $\delta^{15}N$ signal up to 3‰ due to changes in trophic level.

References

Adams, T. S., & Sterner, R. W. (2000). The effect of dietary nitrogen content on trophic level ^{15}N enrichment. *Limnology and Oceanography, 45*, 601-607.

Ander, J. (1997). Volcanic History of the Northern Chain of Craters. In: K. Mabery (Ed.), *Natural History of El Malpais National Monument*. Albuquerque: Authority of State of New Mexico, 31-39.

Andrade, E. R., & Sellers, W. D. (1988). El Niño and its effect of precipitation in Arizona and Western New Mexico. *Journal of Climatology, 8*, 403-410.

Andres, R. J., Marland, G., Boden, T., & Bischof, S. (1996). Carbon dioxide emissions from fossil fuel consumption and cement manufacture, 1751 to 1991, and an estimate of their isotopic composition and latitudinal distribution, in The Carbon Cycle (Wigley, T. M. L., ed.), Cambridge Univ. Press, New York.

Aquatic Research Instruments (n.d.). Retrieved 2018, from http://www.aquaticresearch.com/news.htm

Asmerom, Y., Polyak, V., Burns, S., & Rassmussen, J. (2007). Solar forcing of Holocene climate: New insights from a speleothem record, southwestern United States. *Geology, 35*, 1-4.

Austin, A. T., & Vitousek, P. M. (1998). Nutrient dynamics on a precipitation gradient in Hawaii. *Oecologia, 113*, 519-529.

Bird, M. I., Boobyer, E. M., Bryant, C., Lewis, H. A., Paz, V., & Stephens, W. E. (2007). A long record of environmental change from bat guano deposits in Makangit Cave, Palawan,

Philippines. *Earth and Environmental Science Transactions of the Royal Society of Edinburgh, 98*, 59-69.

Blaauw, M. (2010). Methods and code for 'classical' age-modelling of radiocarbon sequences. *Quaternary Geochronology, 5*, 512-518.

Bleakly, D. L. (1997). Plantlife on the lava-The vegetation and flora of El Malpais. *New Mexico Bureau of Mines & Mineral Resources, 156*, 113-122.

Bradley, R. S., Diaz, H. F., Kiladis, G. N., & Eischeid, J. K. (1987). ENSO signal in continental temperature and precipitation records. *Nature, 327*, 497-501.

Bradley, R. S. (2015). *Paleoclimatology: Reconstructing climates of the Quaternary* (3rd ed.). Academic Press, San Diego, 696 p.

Bryson, R. A., & Lowry, W. P. (1955). The synoptic climatology of the Arizona summer precipitation singularity. *Bulletin of the American Meteorological Society, 36*, 329-339.

Carrillo, C. M., Castro, C. L., Chang, H. I., & Luong, T. M. (2017). Multi-year climate variability in the Southwestern United States within a context of a dynamically downscaled twentieth century reanalysis. *Climate Dynamics, 49*, 4217-4236.

Cerling, T. E., Harris, J. M., MacFadden, B. J., Leakey, M. G., Quade, J., Eisenmann, V., & Ehleringer, J. R. (1997). Global vegetation change through the Miocene-Pliocene boundary. *Nature, 389*, 153-158.

Citterio, M., Turri, S., Bini, A., & Maggi, V. (2004). Observed trends in the chemical composition, $\delta^{18}O$ and crystal sizes vs. depth in the first ice core from the "LoLc 1650 Abisso sul Margine dell'Alto Bregai" ice cave (Lecco, Italy). *Theoretical and Applied Karstology, 17*, 45-50.

Clark, I., & Fritz, P. (1997). *Environmental Isotopes in Hydrology.* Boca Raton: CRC Press, 328 p.

Cleary, D. M., Onac, B. P., Forray, F. L., & Wynn, J. G. (2016). Effect of diet, anthropogenic activity, and climate on δ^{15}N values of cave bat guano. *461*, 87-97.

Craig, H. (1961). Isotopic Variation in Meteoric Waters. *Science, 133*, 1702-1703.

Dansgaard, W. (1964). Stable isotopes in precipitation. *Tellus, 16*, 436-468.

Davidson, E. A., Carvalho, C. J. R., Figueira, A. M., Ishida, F. Y., Ometto, J. P. H. B., Nardoto, G. B., Sabá, R. T., Hayashi, S. N., Leal, E. C., Vieira, I. C. G., & Martinelli, L. A. (2007). Recuperation of nitrogen cycling in Amazonian forests following agricultural abandonment. *Nature, 447,* 995-998.

Davies, M. J. (1959). A contribution to the ecology of species of *Notiophilus* and allied genera (Col., Carabidae). *Entomologist's Monthly Magazine, 95*, 25-28.

Davis, R. B., Herreid, C. F., & Short, H. R. (1962). Mexican Free-Tailed Bats in Texas. *Ecological Monographs, 32*, 311-346.

De Niro, M. J., & Epstein, S. (1978). Influence of diet on the distribution of carbon isotopes in animals. *Geochimica et Cosmochimica Acta, 42*, 495-506.

Dickfoss, P. V. (1996). *Stratified ice accumulations as a source of climate proxy data.* Ohio State University, 220 p.

Dickfoss, P. V., Betancourt, J. L., Thompson, L. C., Turner, R. M., & Tharnstrom, S. (1997). History of ice at Candelaria Ice Cave. In K. Mabery (Eds.), *Natural History of El Malpais National Monument*. Albuquerque: Authority of State of New Mexico, 91-112.

Dunbar, N. W., & Phillips, F. M. (1994). *36-Cl* surface exposure determinations of eruption ages for Quaternary flows of the Zuni-Bandera volcanic field. *New Mexico Bureau of Geology & Mineral Resources Bulletin, 160,* 309-317.

Ehleringer, J. R., Cerling, T. E., & Helliker, B. R. (1997). C_4 photosynthesis, atmospheric CO_2,
and climate. *Oecologia, 112*, 285-299.

Ellsworth, P., Feldman, M., Baxter, I. & Cousins, A. (2001). A genetic link between whole-plant
water use efficiency and leaf carbon isotope composition in the C_4 grass *Setaria*
(pre-print). *bioRxiv,* 1-32.

Evans, R. D. (2001, March). Physiological mechanisms influencing plant nitrogen isotope
composition. *Trends in Plant Science, 6*, 121-126.

Farquhar, G. D., O'Leary, M. H., & Berry, J. A. (1982). On the Relationship between Carbon
Isotope Discrimination and the Intercellular Carbon Dioxide Concentration in Leaves.
Australian Journal of Plant Physiology, 9, 121-137.

Follett, R. F., Kimble, J., Leavitt, S. W. & Pruessner, E. 2004. Potential use of soil C isotope
analyses to evaluate paleoclimate. *Soil Science, 169*, 471-488.

Forray, F. L., Onac, B. P., Tanţău, I., Wynn, J. G., Tămaş, T., Coroiu, I., & Giurgiu, A. M.
(2015). A Late Holocene environmental history of a bat guano deposit from Romania: an
isotopic, pollen and microcharcoal study. *Quaternary Science Reviews, 127*, 141-154.

Froehlich, K., Gibson, J. J., & Aggarwal, P. (2002). *Deuterium excess in precipitation and its
climatological significance.* Vienna: International Atomic Energy Agency, 2-23.

Fórizs, I., Kern, Z., Szántó, Z., Nagy, B., Palcsu, L., & Molnár, M. (2004). Environmental
isotopes study on perennial ice in the Focul Viu ice cave, Bihor Mountains, Romania.
Theoretical and Applied Karstology, 17, 61-69.

Galloway, J. N., Dentener, F. J., Capone, D. G., Boyer, E. W., Howarth, R. W., Seitzinger, S. P.,
Asner, G.P., Cleveland, C.C., Green, P.A., Holland, E.A., Karl, D.M., Michaels, A.F.,

Porter, J.H., Townsend, A.R., & Vörösmarty, C. (2004). Nitrogen cycles: past, present, and future. *Biogeochemistry, 70*, 153-226.

Galloway, J. N., Schlesinger, W. H., Levy II, H., Michaels, A., & Schnoor, J. L. (1995). Nitrogen fixation: Anthropogenic enhancement-environmental response. *Global Biogeochemical Cycles, 9*, 235-252.

Garfin, G., Franco, G., Blanco, H., Comrie, A., Gonzalez, P., Piechota, T., Smyth, R., & Waskom, R. (2014). *Climate Change Impacts in the United States: The Third National Climate Assessment.* Washington D.C.: U.S. Global Change Research Program.

Gat, J. R. (2010). *Isotope Hydrology: A Study of the Water Cycle.* London: Imperial College Press, 6, 189 p.

Glover, V.J., & Hereford, Jr., J.P. 1986. *Zuni Mountain Railroads Cibola Nation- al Forest, New Mexico.* USDA Forest Service *Cultural Resources Management, Report 6,* pp. 87

Greeley, R. (1987). The role of lava tubes in hawaiian volcanoes. In: R. Decker, T. Wright, & P. Stauffer (eds.), *Volcanism in Hawaii: U.S. Geological Survey Professional Paper 1350.* USGS, 1589-1602

Grissino-Mayer, H. D. (1995). *The climate and fire history of El Malpais National Monuments.* Tuscon: The University of Arizona, 407 p.

Gruber, N., & Galloway, J. N. (2008). An Earth-system perspective of the global nitrogen cycle. *Nature, 451*, 293-296.

Högberg, P. (1997). ^{15}N natural abundance in soil-plant systems. *New Phytologist, 137*, 179-203.

Hales, J. E. (1974). Southwestern United States Monsoon Source - Gulf of Mexico or Pacific Ocean. *Journal of Applied Meteorology*, 331-342.

Handley, L., Austin, A., Robinson, D., Scrimgeour, C., Raven, J., Heaton, T., Schmidt, S., & Stewart, G. (1999). The ^{15}N natural abundance (δ^{15}N) of ecosystem samples reflects measures of water availability. *Australian Journal of Plant Physiology, 26*, 185-199.

Hatch, M. D., Slack, C. R., & Johnson, H. S. (1966). Further Studies on a New Pathway of Photosynthetic Carbon Dioxide Fixation in Sugar-Cane and its Occurrence in other Plant Species. *Biochemical Journal., 102*, 417-422.

Hass, C. H. (1996) Northern Europe climate variations during late Holocene: evidence from marine Skagerrak. *Palaeogeography, Palaeoclimatology, Palaeoecology, 123,* 121-145.

Herreid, C. F. II. (1959). Sexual Dimorphism in Teeth of the Free Tailed Bat. *Journal of Mammology, 40,* 538-541.

Higgens, R. W., Yao, Y., & Wang, X. L. (1997). Influence of the North American Monsoon System on the U.S. Summer Precipitation Regime. *Journal Of Climate, 10*, 2600-2622.

Higgins, R. W., & Shi, W. (2000). Dominant Factors Responsible for Interannual Variability of the Summer Monsoon in the Southwestern United States. *Journal of Climate, 13*, 759-766.

Higgins, R. W., Mo, K. C., & Yao, Y. (1998). Interannual variability of the United States summer precipitation regime with emphasis on the southwestern monsoon. *Journal Of Climate, 11*, 2582-2606.

Hobbie, E. A., Macko, S. A., & Williams, M. (2000). Correlations between foliar δ^{15}N and nitrogen concentrations may indicate plant-mycorrhizal interactions. *Oecologia, 122*, 273-283.

Hoy, R. N., & Gross, G. W. (1982). *Baseline study of oxygen 18 and deuterium in the Roswell, New Mexico, groundwater basin.* Technical Report, New Mexico Water Resources Research Institute, 95 p.

IAEA, & UNESCO. (2001). *Environmental Isotopes in the Hydrological Cycle.* IAEA, UNESCO.

Kauahikaua, J., Kashman, K. V., Mattox, T. N., Heliker, C. C., Hon, K. A., Mangan, M. T., & Thornbet, C. R. (1998). Observations on basaltic lava streams in tubes from Kilauea Volcano, island of Hawai'i. *Journal of Geophysical Research, 103*, 303-327.

Keeling, C. D., Mook, W. G., & Tans, P.P. (1979) Recent trends in the $^{13}C/^{12}C$ ratio of atmospheric carbon dioxide. *Nature, 277*, 121-123.

Kelly, J. F. (2000, February). Stable isotopes of carbon and nitrogen in the study of avian and mammalian trophic ecology. *Canadian Journal of Zoology, 78*, 1-27.

Kendall, C., Elliott, E. M., & Wankel, S. D. (2007). Tracing anthropogenic inputs of nitrogen to ecosystems, Chapter 12. In: R. H. Michener, & K. Lajtha, *Tracing anthropogenic inputs of nitrogen to ecosystems* (2nd ed.). Oxford: England Blackwell Publishing, 566 p.

Kern, Z., Fórizs, I., Nagy, B., Kázmér, M., Gál, A., Szántó, Z., Palcsu, L., & Molnár, M. (2004). Late Holocene environmental changes recorded at Ghețarul de la Focul Viu Ice Cave, Bihor Mountains, Romania. *Theoretical and Applied Karstology, 17*, 51-60.

Kiladis, G. N., & Diaz, H. F. (1989). Global climate anomalies associated with extremes of the Southern Oscillation. *Journal of Climate, 2*, 1069-1090.

Lachniet, M. S. (2009). Climatic and environmental controls on speleothem oxygen-isotope values. *Quaternary Science Reviews, 28*, 412-432.

Lachniet, M. S., Bernal, J. P., Asmerom, Y., Polyak, V., & Piperno, D. (2012). A 2400 yr Mesoamerican rainfall reconstruction links climate and cultural change. *Geology, 40*, 259-262.

Lamb H. H. (1982) The Climatic Environment of the Arctic Ocean. In: Rey, L. (Eds.) The Arctic Ocean. Palgrave Macmillan, London, 135-161.

Lamb H. H. (1995) Climate History and the Modern World (2nd ed.). New York: Routledge.

Lambers, H., Chapin, F. S., & Pons, T. L. (2008). Plant Water Relations. *Plant Physiological Ecology, 1*, 163-223.

Laughlin, A. W., Perry, F. V., Damon, P. E., Shafiqullah, M., WoldeGabriel, G., McIntosh, W., Harrington, C.D., Wells, S.G., & Drake, P. (1993). Geochronology of Mount Taylor, Cebollita Mesa, and Zuni-Bandera volcanic fields, Cibola County, New Mexico. In *New Mexico Geology, 15*, 82-93.

Laughlin, A. W., Poths, J., Healey, H. A., Reneau, S., & WoldeGabriel, G. (1994). Dating of Quaternary basalts using the cosmogenic 3-He and 14-C methods with implications for excess 40-Ar. *Geology, 22*, 135-138.

Libby, W. F. (1955). *Radiocarbon dating* (2nd ed.). University of Chicago Press, 175 p.

Ljungqvist, F. C. (2010). A new reconstruction of temperature variability in the extra-tropical Northern Hemisphere during the last two millennia. *Physical Geography, 92A,* 339-351.

Lowe, J., & Walker, M. (2015). *Reconstructing Quaternary Environments* (2nd ed.). New York: Routledge, 538 p.

Luetscher, M., Jeannin, P., & Haeberli, P. W. (2005). Ice caves as an indicator of winter climate evolution: a case study from the Jura Mountains. *The Holocene, 15*, 982-993.

Ma, J. Y., Sun, W., Liu, X. N., & Chen, F. H. (2012). Variation in the stable carbon and nitrogen isotope composition of plants and soil along a precipitation gradient in northern China. *PLoS ONE, 7,* 1-7.

Mabery, K. (1997). *Natural History of El Malpais National Monument.* Albuquerque, NM:

   Authority of State of New Mexico.

Marais, D. J., Mitchell, J. M., Meinshein, W. G., & Hayers, J. M. (1980). The carbon isotope

   biogeochemistry of the individual hydrocarbons in bat guano and the ecology of the

   insectivorous bats in the region of Carlsbad, New Mexico. *Geochimica et Cosmochimica*

   Acta, 44, 2075-2086.

Maxwell, W. C. (1986). *Geologic map of El Malpais lava field and surrounding areas, Cibola*

   County, New Mexico. US Geological Survey.

McGrath, D. A., Smith, C. K., Gholz, H. L. & Oliveira, F. A. (2001). Effects of land-use change

   on soil nutrient dynamics in Amazônia. *Ecosystems, 4,* 625-645.

Merlivat, L., & Jouzel, J. (1979). Global climatic interpretation of the deuterium-oxygen 18

   relationship for precipitation. *Journal of Geophysical Research, 84*, 5029-5033.

Mitchell, J. M. (1972). *The geochemical significance of the alkanes in bat guano.* Bloomington,

   IN: Indiana University.

NASA (2018). *NASA Earth Observatory*. Retrieved from

   https://earthobservatory.nasa.gov/Features/CarbonCycle

NOAA (2012). *Pacific/North American (PNA)*. Retrieved from National Weather Service:

   Climate Prediction Center: http://www.cpc.ncep.noaa.gov/data/teledoc/pna.shtml

NOAA (2017). *Carbon Tracker CT2017*. Retrieved from noaa.gov:

   https://www.esrl.noaa.gov/gmd/ccgg/carbontracker/

NOAA (2018). *Climate at a Glance*. Retrieved from ncdc.noaa.gov:

   https://www.ncdc.noaa.gov/cag/

NOAA (2018). *Find a Station: Albuquerque.* Retrieved from ncdc.noaa.gov:

    https://www.ncdc.noaa.gov/cag/

NPS (2015a). *El Malpais National Monument Caving Brochure.* Retrieved from nps.gov:

    https://www.nps.gov/elma/learn/nature/upload/Caving-brochure-july-2015.pdf

NPS (2015b). *Weather.* Retrieved from El Malpais National Monument:

    https://www.nps.gov/elma/learn/nature/weather.htm

Ohata, T., Furukawa, T., & Osada, K. (1994). Glacioclimatological Study of Perennial Ice in the

    Fuji Ice Cave Part 2: Interannual Variation and Relation to Climate. *Arctic and Alpine*

    Research, 26, 238-244.

O'Leary, M. H. (1981). Carbon isotope fractionation in plants. *Phytochemistry, 20*, 553-567.

Onac, B. P., Forray, F. L., Wynn, J. G., & Giurgiu, A. M. (2014). Guano-derived δ13C-based

    paleo-hydroclimate record from Gaura cu Muscă Cave, SW Romania. *Environmental*

    Earth Sciences, 71 (9), 4061-4069.

Pendall, E. G. (1997). *Precipitation seasonality recorded in D/H ratios of Pinyon Pine Cellulose*

    in the Southwestern United States. University of Arizona.

Perşoiu, A., & Onac, B. P. (2018). Ice in caves. In W.B. White, & D. Culver, *Encyclopedia of*

    Caves (3rd ed.). Elsevier, in press.

Perşoiu, A., Onac, B. P., Wynn, J. G., Bojar, A., & Holmgren, K. (2011). Stable isotope behavior

    during cave ice formation by water freezing in Scărişoara Ice Cave, Romania. *Journal of*

    Geophysical Research, 116, 1-8.

Perşoiu, A., & Lauritzen, S. E. (2018). *Ice Caves.* Cambridge: Elsevier Inc.

Poage, M. A., & Chamberlain, C. P. (2001). Empirical relationships between elevation and the

    stable isotope composition of precipitation and surface waters: considerations for studies

    of paleoelevation change. *American Journal of Science, 301*, 1-15.

Polyak, V. J., & Asmerom, Y. (2001). Late Holocene Climate and Cultural Changes in the

    Southwestern United States. *Science, 294*, 148-151.

R Development Core Team (2013). (V. A. R Foundation for Statistical Computing, Producer)

    Retrieved from R: A language and environment for statistical computing: http://www.r-

    project.org

Racoviţă, G., & Şerban, M. (1990). Interprétation en vue d'une reconstitution paléoclimatique

    des particularités structurales et dynamiques du dépôt de glace pérenne de la grotte de

    Scărişoara. *StudiaUBB Geologia, 35*, 47-61.

Ralph, C. P. (1976). Natural Food Requirements of the Large Milkweed Bug, Oncopeitus fascia

    tus (Hemiptera: Lygaeidae), and Their Relation to Gregariousness and Host Plant

    Morphology. *Oecologia (Berl.), 26*, 157-175.

Ranson, S. L., & Thomas, M. (1960). Crassulacean Acid Metabolism. *Annual Review of Plant

    Physiology, 11*, 81-110.

Reimer, P. J., & Reimer, R. (2009). *CALIBomb Radiocarbon Calibration*. Retrieved from

    http://intcal.qub.ac.uk/CALIBomb

Reimer, P. J., Bard, E., Bayliss, A., Beck, J. W., Blackwell, P., Bronk Ramsey, C., Buck, C.E.,

    Cheng, H., Edwards, R.L., Friedrich, M., Grootes, P.M., Guilderson, T.P., Haflidason, H.,

    Hajdas, I., Hatte, C., Heaton, T. J., Hoffmann, D. L., Hogg, A. G., Hughen, K. A., Kaiser,

    K.F., Kromer, B., Manning, S.W., Niu, M., Reimer, R.W., Richards, D.A., Scott, E.M.,

    Southon, J.R., Staff, R.A., Turney, C.S.M., & van der Plicht, J. (2013). IntCal13 and

Marine13 radiocarbon age calibration curves 0-50,000 years cal BP. *Radiocarbon, 55*, 1869-1887.

Robinson, D. (2001). $\delta^{15}N$ as an integrator of the nitrogen cycle. *Trends in Ecology & Evolution, 16*, 153-162.

Rogers, B. W., & Mosch, C. J. (1997). In the basement - Lava-tube origins and morphology. In K. Mabery, *Natural History of El Malpais National Monument*. Albuquerque: Authority of State of New Mexico, 61-68.

Rozanski, K. (1987). Deuterium and oxygen-18 in atmospheric part of hydrological cycle. *Scientific Bulletins of Academy of Mining and Metallurgy, 14*, 1-100.

Rozanski, K., Araguas-Araguas, L., & Gonfanttni, G. (1993). Isotopic Patterns in Modern Global Precipitation. (Swart, P., Lohmann, K., Mckenzie, J., & Savin, S., Eds.) *Climate Change in Continental Isotopic Records, Geophysical Monograph Series, 78*, 1-36.

Sage, R. F. (2004). The evolution of C_4 photosynthesis. *New Phytologist, 161*, 341-370.

Schmitz, J. T., & Mullens, S. L. (1996). Water vapor transport associated with the summertime North America Monsoon as Depicted by ECMWF analysis. *Journal of Climate, 9*, 1621-1634.

Scott, R. C. (1991). *Essentials of physical geography.* New York: West Publishing Co.

Sellers, W. D., & Hill, R. H. (1974). *Arizona Climate* (2nd ed.). Tucson: University of Arizona Press.

Şerban, M., Blaga, L., Blaga, L., Chifu, A., & Ciobotaru, T. (1967). Contribuţii la stratigrafia depozitelor de gheaţă din Gheţarul de la Scărişoara. *Lucrările Institutului de Speologie "Emil Racoviţă" 6*, 107-140.

Shackleton, N. (1967). Oxygen isotope analyses and Pleistocene temperatures re-assessed. *Nature, 215*, 15-17.

Sharp, Z. (2007). *Principles of Stable Isotope Geochemistry.* Upper Saddle River, NJ: Pearson
Education.

Sheppard, P. R., Comrie, A. C., Packin, G. D., Angersbach, K., & Hughes, M. K. (1999). *The
Climate of the Southwest.* The University of Arizona. Tucson: Institute for the Study of
Planet Earth.

Silva, L. C., & Horwath, W. R. (2013). Explaining global increases in water use efficiency: why
have we overestimated responses to rising atmospheric CO_2 in natural forest ecosystems?
Plos One, 8, e53089.

Simmons, A. J., Wallace, J. M., & Branstator, G. W. (1983). Barotropic wave propagations and
instability, and atmospheric teleconnections. *Journal of the Amospheric Sciences, 40*,
1363-1393.

Smith, B. N., & Epstein, S. (1971). Two Categories of $^{13}C/^{12}C$ Ratios for Higher Plants. *Plant
Physiology, 47*, 380-384.

Smith, W. (1986). *The Effects of Eastern North Pacific Tropical Cyclones on the Southwestern
United States.* Silver Spring: National Weather Service.

Swap, R. J., Aranibar, J. N., Dowty, P. R., Gilhooly III, W. P., & Macko, S. A. (2004). Natural
abundance of ^{13}C and ^{15}N in C_3 and C_4 vegetation of southern Africa: patterns and
implications. *Global Change Biology, 10*, 350-358.

Taylor, R. E. (1997). Radiocarbon Dating. In R. E. Taylor, & M. J. Aitken, *Chronometric Dating
in Archaeology*, Vol. 2, pp. 65-96. New York: Plenum Press.

Thirumalai, K., Quinn, T. M., Okumura, Y., Richey, J. N., Partin, J. W., Poore, R. Z., & Moreno
Chamarro, E. (2018). Pronounced centennial-scale Atlantic Ocean climate variability
correlated with Western Hemisphere hydroclimate. *Nature Communications, 9*, 1-11.

Thury, M. (1861). Etude des Glacières naturelles. *Archives des sciences de la bibliothèque universelle*, pp. 59.

Tiunov, A. V. (2007). Stable Isotopes of Carbon and Nitrogen in Soil Ecological Studies. *Biology Bulletin, 34*, 395-407.

Trouet, V., Diaz, H. F., Wahl, E. R., Viau, A. E., Graham, R., Graham, N., & Cook, E. R. (2013). A 1500-year reconstruction of annual mean temperature for temperate North America on decadal-to-multidecadal time scales. *Environmental Research Letters, 8*, 1-10.

USGS (2017, May 3). *Geology of National Parks, 3D and Photographic Tours*. Retrieved from usgs.gov: https://3dparks.wr.usgs.gov/elma/

Vitousek, P. M., Aber, J. D., Howarth, R. W., Likens, G. E., Matson, P. A., Schindler, D. W., Schlesinger, W. H., Tilman, D. G. (1997). Human alteration of the global nitrogen cycle: sources and consequences. *Ecological Applications, 7*, 737-750.

Walsh, J., Wuebbles, D., Hayhoe, K., Kossin, J., Kunkel, K., Stephens, G., Thorne, P., Vose, R., Wehner, M., Willis, J., Anderson, D., Doney, S., Feely, R., Hennon, P., Kharin, V., Knutson, T., Landerer, F., Lenton, T., Kennedy, J., & Somerville, R. (2014). Chapter 2: Our Changing Climate. Climate Change Impacts in the United States. In J. Melillo, T. Richmond, & G. Yohe, *The Third National Climate Assessment* (pp. 19-67). US Global Change Research Program.

Whitaker, J. J., Neefus, C., & Kunz, T. (1996). Dietary variation in the Mexican free-tailed bat (Tadarida Brasiliensis Mexicana). *Journal of Mammology, 77*, 716-724.

Wurster, C., McFarlane, D., & Bird, M. (2007). Spatial and Temporal Expression of Vegetation and Atmospheric Variability from Stable Carbon and Nitrogen Isotope Analysis of Bat Guano in the Southern United States. *Geochimica et Cosmochimica Acta, 71*, 3302-3310.

Wurster, C., Munksgaard, N., Zwart, C., & Bird, M. (2015). The biogeochemistry of insectivorous cave guano: a case study from insular Southeast Asia. *Biogeochemistry, 124*, 164-175.

Yan, H., Sun, L., Wang, Y., Huang, W., Qiu, S., & Yang, C. (2011). A record of the Southern Oscillation Index for the past 2,000 years from precipitation proxies. *Nature Geoscience, 4*, 1-4.

Yapp, C. (1985). D/H variations of meteoric waters in Albuquerque, New Mexico, U.S. *Journal of Hydrology, 76*, 63-84.

Yonge, C., & MacDonald, W. (1999). The potential of perennial cave ice in isotope palaeoclimatology. *Boreas, 28*, 357-362.

Appendix A: Data

Table A.1: Isotope results from the Cave 91 ice core.

Depth (cm)	δ^{18}O (‰)	δ^{2}H (‰)	d-excess (‰)
5.00	-8.94	-60.24	11.28
10.00	-10.10	-69.79	11.01
15.00	-11.36	-79.88	11
20.00	-10.12	-72.46	8.5
25.00	-11.82	-84.81	9.75
30.00	-9.45	-64.28	11.32
35.00	-9.08	-61.38	11.26
40.00	-9.31	-62.87	11.61
45.00	-9.90	-67.72	11.48
50.00	-9.55	-64.40	12
55.00	-9.42	-63.75	11.61
60.00	-8.88	-58.83	12.21
65.00	-8.87	-58.94	12.02
70.00	-9.36	-62.28	12.6
75.00	-9.05	-60.64	11.76
80.00	-8.72	-58.12	11.64
85.00	-9.64	-65.18	11.94
90.00	-9.02	-60.88	11.28
95.00	-9.72	-66.09	11.67
100.00	-9.62	-65.53	11.43

Table A.2: Results from the Cave 455 ice core.

Depth (cm)	$\delta^{18}O$ (‰)	δ^2H (‰)	d-excess (‰)
6	-7.62	-52.26	8.7
8	-9.71	-68.19	9.49
10	-8.78	-63.32	6.92
12	-8.9	-62.77	8.43
14	-8.27	-60.11	6.05
16	-9.08	-64.53	8.11
18	-9.59	-67.87	8.85
20	-9.76	-69.17	8.91
22	-9.82	-69.99	8.57
24	-9.13	-65.85	7.19
26	-8.81	-63.82	6.66
28	-9.06	-65.23	7.25
30	-8.74	-65.49	4.43
32	-9.02	-64.17	7.99
34	-9.54	-67.56	8.76
36	-11.37	-80.75	10.21
38	-12.13	-86.42	10.62
40	-12.22	-87.78	9.98
42	-12.08	-87.39	9.25
44	-12.45	-91.42	8.18
46	-12.19	-90.02	7.5
48	-11.04	-79.63	8.69
50	-9.24	-64.28	9.64
52	-7.97	-53.04	10.72
54	-7.64	-50.09	11.03
56	-8.41	-56.59	10.69
58	-8.63	-58.49	10.55
60	-8.51	-58.21	9.87
62	-8.3	-56.64	9.76
64	-8.47	-58.1	9.66
66	-8.4	-58.28	8.92
68	-8.31	-57.92	8.56
70	-8.6	-59.63	9.17
72	-9.12	-63.09	9.87
74	-9.11	-63.21	9.67
76	-9.03	-62.14	10.1

78	-8.97	-61.85	9.91
80	-8.58	-58.96	9.68
82	-7.6	-55.76	5.04
84	-8.9	-61.83	9.37
86	-8.68	-60.05	9.39
88	-8.97	-62.18	9.58
90	-9.52	-66.04	10.12
92	-9.03	-62.34	9.9
94	-8.6	-59.05	9.75
96	-8.11	-55.73	9.15
98	-8.42	-58.1	9.26
100	-9.4	-65.41	9.79
102	-10.23	-72.63	9.21
104	-10.27	-73.03	9.13
106	-9.7	-71.27	6.33
108	-10.01	-71.01	9.07
110	-8.56	-59.39	9.09
112	-8.34	-57.76	8.96
114	-8.04	-55.46	8.86
116	-11.38	-84.55	6.49
118	-10.09	-73.45	7.27
120	-10.29	-74.1	8.22
122	-10.77	-77.53	8.63
124	-11.36	-82.41	8.47

Table A.3: Cave 29 ice core results. Ages obtained only between 0 and 57 cm depth.

Depth (cm)	Age (AD)	δ^{18}O (‰)	δ^{2}H (‰)	d-excess (‰)
1.00	948	-6.51	-38.97	13.11
2.00	943	-6.43	-38.31	13.13
3.00	933	-6.66	-39.58	13.7
4.00	928	-6.72	-39.95	13.81
6.50	919	-6.63	-40.17	12.87
7.50	914	-6.55	-39.38	13.02
8.50	909	-6.67	-40.43	12.93
9.50	904	-6.82	-41.50	13.06
10.50	899	-6.95	-42.83	12.77
11.50	895	-7.23	-44.17	13.67
14.50	885	-7.32	-45.47	13.09
16.50	857	-7.62	-46.84	14.12
17.50	839	-7.87	-48.38	14.58
19.00	821	-8.00	-49.19	14.81
20.00	784	-8.07	-49.55	15.01
22.00	766	-8.36	-51.23	15.65
23.00	748	-8.15	-49.94	15.26
24.00	711	-8.54	-52.74	15.58
25.00	693	-8.56	-53.91	14.57
26.00	675	-8.62	-54.25	14.71
27.00	657	-8.83	-55.80	14.84
28.00	639	-8.69	-54.36	15.16
30.00	621	-8.47	-52.33	15.43
32.50	586	-8.33	-51.65	14.99
35.00	532	-8.06	-49.70	14.78
37.00	496	-8.47	-52.35	15.41
39.00	460	-7.97	-48.97	14.79
40.50	425	-7.69	-47.33	14.19
42.00	407	-7.60	-46.75	14.05
44.50	371	-7.76	-46.88	15.2
46.00	335	-7.61	-46.24	14.64
47.50	299	-7.56	-46.11	14.37
48.50	282	-7.65	-46.75	14.45
50.00	264	-7.60	-48.09	12.71
51.50	228	-7.81	-46.52	15.96
53.00	210	-7.61	-46.24	14.64

55.00	174	-7.70	-49.14	12.46
57.00	138	-7.53	-47.93	12.31
60.00	N/A	-6.88	-39.42	15.62
65.00	N/A	-7.83	-47.43	15.21
70.00	N/A	-8.23	-50.45	15.39
75.00	N/A	-8.06	-48.30	16.18
80.00	N/A	-7.14	-43.76	13.36
85.00	N/A	-7.07	-39.61	16.95
90.00	N/A	-6.68	-36.27	17.17
95.00	N/A	-5.71	-31.83	13.85
100.00	N/A	-5.79	-28.73	17.59

Table A.4: Bat Cave guano core results. (Clam interpolated ages adjusted using formula discussed in section 3.3.3)

Depth (cm)	Age (AD)	δ¹³C (‰)	Suess Corrected δ¹³C (‰)	δ¹⁵N (‰)
0	2005.26	-16.09	-14.32	8.48
2	2004.75	-17.92	-16.14	8.40
4	2004.66	-19.49	-17.72	6.87
6	2004.57	-19.50	-17.73	7.12
8	2004.48	-19.81	-18.03	8.80
10	2004.38	-18.98	-17.20	7.12
12	2004.29	-18.38	-16.60	7.59
14	2003.78	-18.02	-16.24	8.71
16	2003.69	-19.57	-17.85	8.26
18	2003.60	-14.08	-12.37	8.49
20	2003.51	-17.39	-15.68	8.09
22	2003.41	-18.67	-16.95	6.35
24	2002.49	-15.37	-13.66	5.64
26	2001.57	-16.72	-15.01	8.24
28	2000.64	-15.71	-14.00	6.77
30	1999.72	-18.53	-16.85	7.41
32	1998.79	-18.68	-17.01	7.29
34	1998.29	-16.72	-15.04	8.45
36	1989.69	-16.92	-15.51	8.48
38	1981.51	-16.22	-14.96	7.87
40	1973.33	-15.99	-15.04	6.07
42	1964.73	-15.80	-15.13	6.59
44	1956.55	-12.15	-11.63	5.71
46	1956.41	-16.00	-15.48	7.66
48	1956.27	-12.45	-11.93	6.06
50	1955.80	-16.51	-15.98	6.72
52	1955.76	-15.80	-15.28	6.03
54	1955.71	-14.25	-13.72	7.20
56	1955.65	-13.91	-13.39	8.26
58	1955.61	-13.69	-13.17	8.26
60	1955.55	-16.45	-15.93	7.87
62	1691.31	-15.55	-15.55	8.50
64	1561.64	-16.31	-16.31	8.07
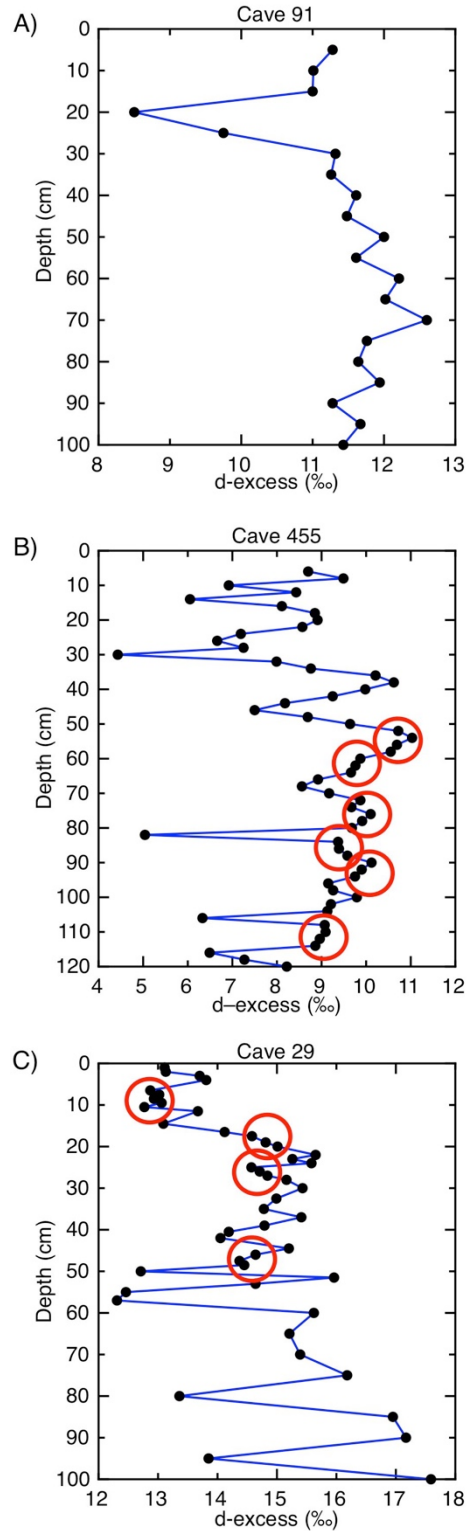
Figure A.1: d-excess plotted against depth for Cave 91 (A), Cave 455 (B), and Cave 29 (C). Red circles denote

clusters of values.
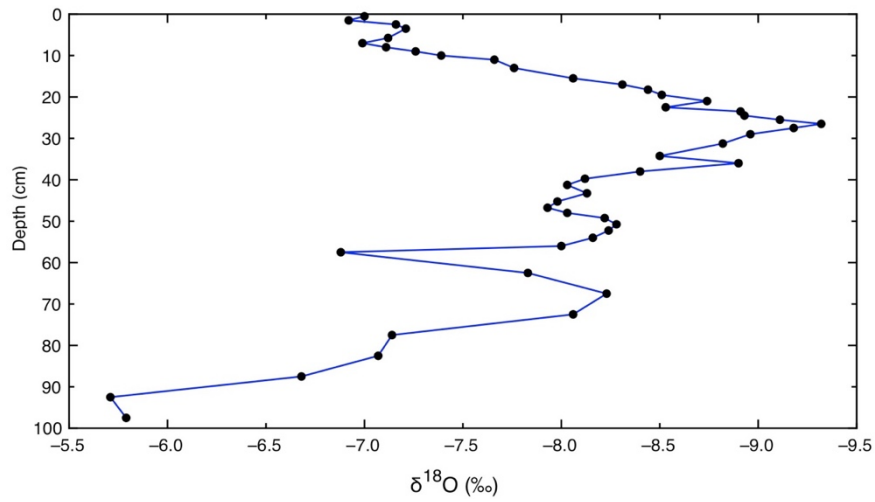
Figure A.2: The $\delta^{18}O$ values plotted against depth for the entire Cave 29 core.
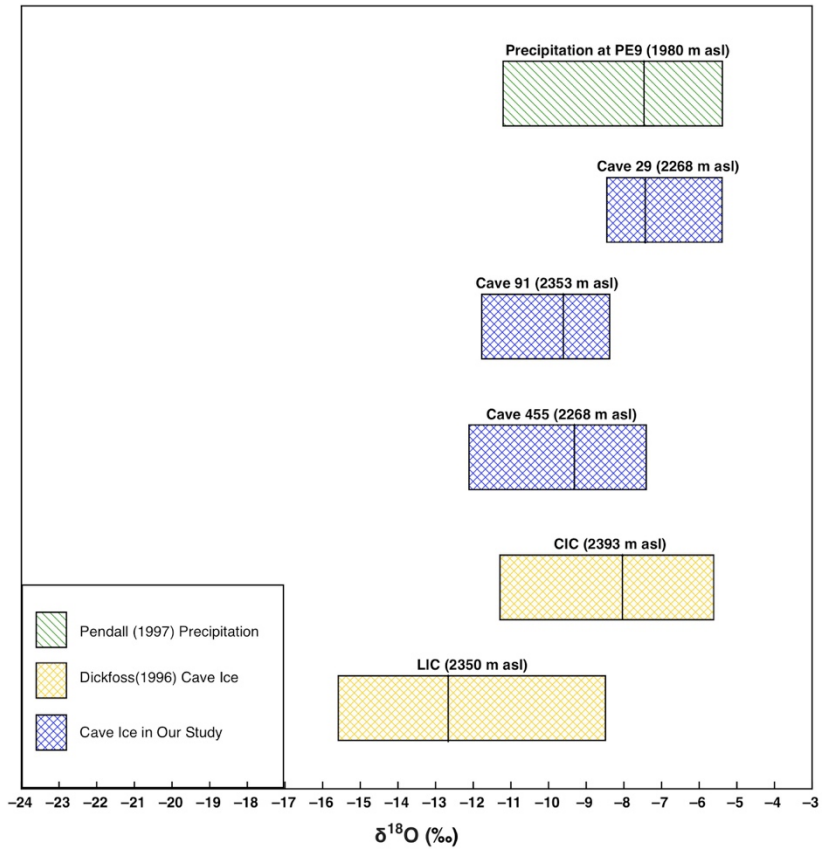
Figure A.3: A box-plot comparison of oxygen isotopes in El Malpais cave ice (including results from this study) and precipitation (Dickfoss, 1996; Pendall 1997) (PE9 = Precipitation; CIC = Candelaria Ice Cave; LIC = La Marchantia Ice Cave)
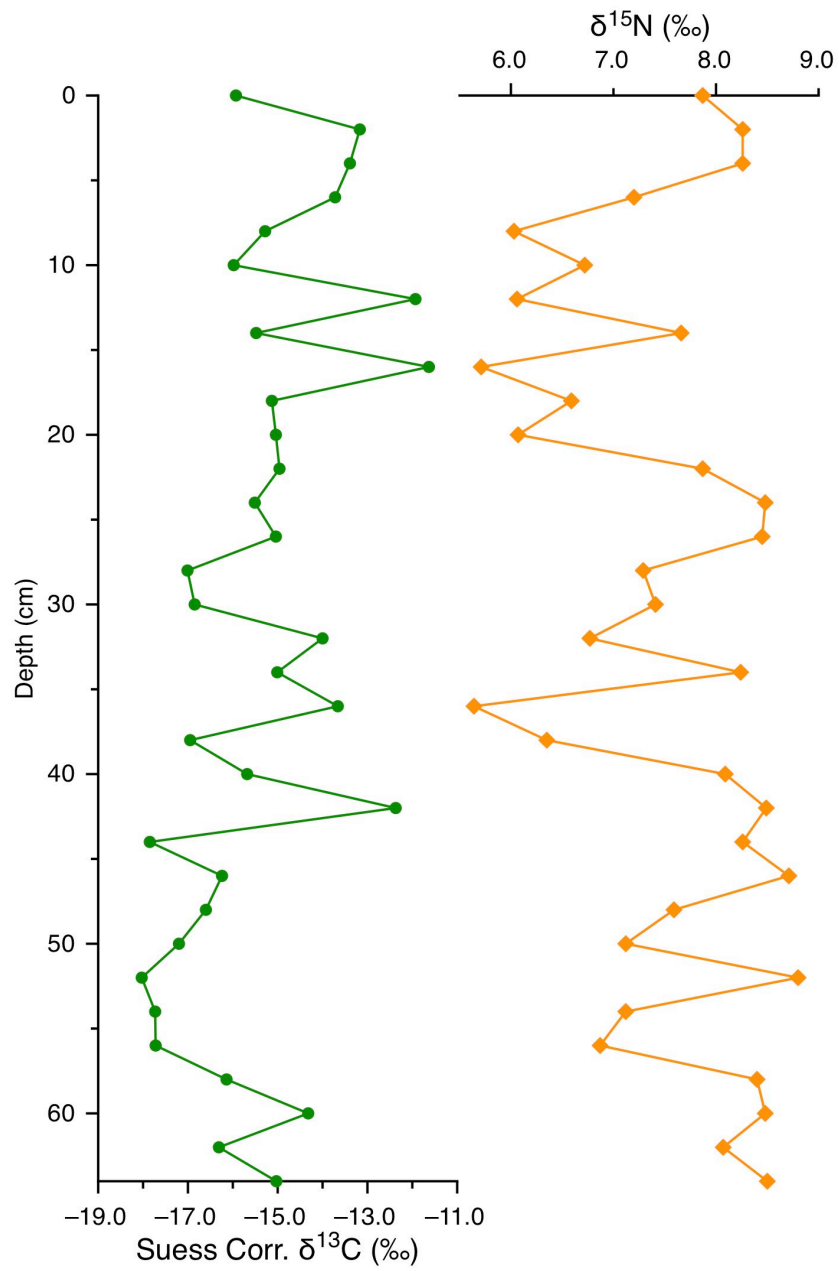
Figure A.4: Carbon and Nitrogen isotopes plotted against depth for the Bat Cave guano core (hiatus only included in the age-depth time series).

Appendix B: Permissions

Figure B.1: Permission granted by Springer Nature for use of figure originally printed in; An Earth-system perspective of the global nitrogen cycle.

Figure B.2: Permission granted by Elsevier for use of figure originally printed in; Climatic and environmental controls on speleothem oxygen-isotope values.

**SPRINGER NATURE LICENSE
TERMS AND CONDITIONS**

Jul 27, 2018

This Agreement between University of South Florida -- Dylan Parmenter ("You") and Springer Nature ("Springer Nature") consists of your license details and the terms and conditions provided by Springer Nature and Copyright Clearance Center.

License Number	4397411309603
License date	Jul 27, 2018
Licensed Content Publisher	Springer Nature
Licensed Content Publication	Climate Dynamics
Licensed Content Title	Multi-year climate variability in the Southwestern United States within a context of a dynamically downscaled twentieth century reanalysis
Licensed Content Author	Carlos M. Carrillo, Christopher L. Castro, Hsin-I Chang et al
Licensed Content Date	Jan 1, 2017
Licensed Content Volume	49
Licensed Content Issue	11
Type of Use	Thesis/Dissertation
Requestor type	academic/university or research institute
Format	print and electronic
Portion	figures/tables/illustrations
Number of figures/tables/illustrations	1
Will you be translating?	no
Circulation/distribution	<501
Author of this Springer Nature content	no
Title	Ice and Guano Deposits in El Malpais Lave Tubes: Potential paleoclimate archives for the Southwest United States
Instructor name	Dr. Bogdan Onac
Institution name	University of South Florida
Expected presentation date	Oct 2018
Portions	Figure 2 (bottom) on page 4223. JA MFC anomaly time series
Requestor Location	University of South Florida 4202 E. Fowler Ave. TAMPA, FL 33620 United States Attn: Dylan Parmenter
Billing Type	Invoice
Billing Address	University of South Florida 4202 E. Fowler Ave.

Figure B.3: Permission granted by Springer Nature for use of figure originally printed in; Multi-year climate variability in the Southwestern United States within a context of dynamically downscaled twentieth century reanalysis.